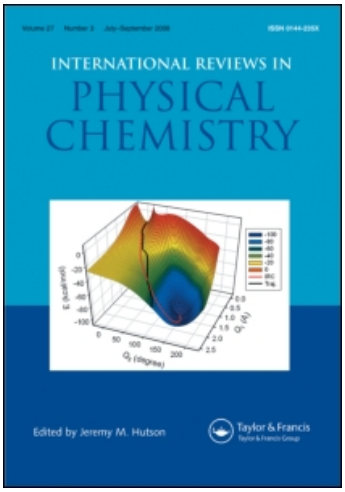

International Reviews in Physical Chemistry
Publication details, including instructions for authors and subscription information:
http://www.informaworld.com/smpp/title~content=t713724383

Non-adiabatic effects in chemistry revealed by time-resolved charged-particle imaging

Toshinori Suzuki; Benjamin J. Whitaker

Online publication date: 26 November 2010

To cite this Article Suzuki, Toshinori and Whitaker, Benjamin J.(2001) 'Non-adiabatic effects in chemistry revealed by time-resolved charged-particle imaging', International Reviews in Physical Chemistry, 20: 3, 313 — 356
To link to this Article: DOI: 10.1080/01442350110045046
URL: http://dx.doi.org/10.1080/01442350110045046

INT. REVIEWS IN PHYSICAL CHEMISTRY, 2001, VOL. 20, NO. 3, 313–356

Non-adiabatic effects in chemistry revealed by time-resolved charged-particle imaging

TOSHINORI SUZUKI and BENJAMIN J WHITAKER†

Institute for Molecular Science and Graduate University for Advanced Studies, Myodaiji, Okazaki 444-8585, Japan

Recent advances in photoelectron and photoion imaging techniques are reviewed. The general background to photofragmentation spectroscopy and, in particular, the information that can be extracted from laboratory and molecular frame photoproduct angular distributions are briefly discussed. Recent technological advances to the photofragment imaging experiment first introduced by Chandler and Houston, such as velocity mapping and event counting, are also described. The main focus of the review is devoted to time-resolved imaging applications in which femtosecond pump–probe techniques are combined with charged particle imaging. We survey the recent literature and describe a number of applications; in particular we show how pump–probe photoelectron imaging can be used to follow intersystem crossing in molecules such as pyrazine, and we also show how the transfer of nuclear coherences can be followed with this technique. We discuss how time-resolved pump–probe photofragment imaging can be used to follow unimolecular decomposition of free radicals with small reaction barriers and we show how this can lead to non-statistical behaviour as a result of restricted rovibrational coupling. Finally, we describe recent applications of pump–probe Coulomb explosion imaging which has the potential to image directly the nuclear wavefunction throughout the course of a chemical reaction. The review closes with some brief conclusions and pointers for future work.

Contents

† On leave from School of Chemistry, University of Leeds, Leeds LS2 9JT, UK. E-mail: benw@chem.leeds.ac.uk

International Reviews in Physical Chemistry ISSN 0144–235X print/ISSN 1366–591X online © 2001 Taylor & Francis Ltd
http://www.tandf.co.uk/journals
DOI: 10.1080/01442350110045046

1. Introduction

Chemistry is concerned with the transformation of one substance into another, and chemists have invented a wealth of strategies to influence the pathways by which reactions occur: controlling the reaction environment, temperature, pH, etc. To understand (and hopefully to direct) the outcome of a particular reaction the chemist pictures a 'mechanism' that is based on the underlying molecular structure of the reagents and products. This concept is central to our general understanding of inorganic, organic and biochemical reactions. At its heart is a special configuration of atoms, known as the transition state, which marks the boundary between what is identifiably reagent and what is product. Factors that influence the nuclear configuration close to the transition state therefore, clearly, have a profound influence on why some chemistry 'happens' and why some does not. The study of these factors is the realm of molecular dynamics.

Among the most recently developed experimental tools for probing these dynamics is charged particle imaging (CPI). The aim of the experiment is to measure the speed and directional distribution of quantum-state-resolved product species following some initiating event, such as the absorption of a photon or a bimolecular collision. By determining the internal energy partitioning in the products, which can be deduced from their speed distribution by conservation of energy, together with the angular distribution, one can infer a great deal about the dynamics involved. For example, consider the case of photodissociation of a triatomic molecule, $ABC + h\nu \rightarrow A + BC$. By conservation of energy, the excess energy between the absorbed photon and the bond energy, $\varepsilon = h\nu - D_0$, must be divided between the relative translation of the photofragments (recoil velocity) and the internal (vibrational and rotational) modes of the diatomic moiety. On statistical (Boltzmann) grounds, one expects (Levine and Bernstein 1987) the relative fractions in translation, rotation and vibration to be $\langle f_t \rangle = \frac{3}{7}$, $\langle f_r \rangle = \frac{2}{7}$ and $\langle f_v \rangle = \frac{2}{7}$ respectively. Any deviation from these 'prior' values implies the intervention of some sort of dynamical influence in the dissociation process. For example, the observation of rotational excitation, that is $\langle f_r \rangle > \frac{2}{7}$, in the diatomic photofragment results from a bent photoexcited state in which a torque is exerted as the unstable ABC* molecule dissociates (Bersohn 1984). A classic example of this behaviour is to be found in the 157 nm photolysis of water (Andresen and Rothe 1983). By contrast, 157 nm photodissociation of the linear OCS molecule is found to lead to highly vibrationally excited CO with virtually no rotational excitation (Ondrey *et al.* 1983). This can be understood if we imagine the CO bond length in the excited OCS molecule to be far from its equilibrium position. As the OCS dissociates, the CO bond relaxes, like a released spring, and vibrational excitation is observed in consequence. Almost no rotational excitation is observed because the transition state is linear in this case.

More pertinently to the subject of this article, the time scale of the dissociation can be inferred from the angular distribution of the photofragments (see for example Bush and Wilson (1972) and Bersohn (1975)). If the photolysing light is linearly polarized, one generally finds a correlation between the recoil velocity $\mathbf{v}$ and the polarization vector $\mathbf{E}$. This arises because the absorption probability is proportional to the square of the scalar product of the transition dipole moment μ and $\mathbf{E}$. If the molecular dissociation is fast with respect to the rotation of the nuclear framework the vector correlation between $\mathbf{E}$ and μ is carried over into the recoil velocity. So, in the case of a diatomic molecule dissociating via a parallel transition the most probable recoil direction is proportional to $\cos^2 \vartheta$, where ϑ is the angle between μ

and **E**. The degree of correlation between the directions of **E** and **v** is therefore reflected in the photoproduct angular distribution (PAD) and is controlled by the time scale of the dissociation with respect to the rotational period of the parent molecule. The angular distribution is given by an expression developed first by Yang (1948) to describe photoionization and then later by Zare (1972) in the context of photofragmentation (see also Bersohn and Lin (1969)):

$$I(\vartheta) = \frac{\sigma}{4\pi}[1 + \beta P_2(\cos\vartheta)], \tag{1}$$

where $P_2(x)$ is the second order Legendre polynomial $\frac{1}{2}\left(3x^2 - 1\right)$ and σ is the total photolysis cross-section.

The parameter β characterizes the anisotropy of the PAD. At this point we note, and shall come back to later, an important difference between PADs measured in different reference frames. For example, in the case of atomic photoionization there is no body-fixed axis system, since the atom is spherically symmetric, and only the polarization vector of the light (in the laboratory frame) gives an axis of reference for the photoelectrons. For molecular photofragmentation and ionization, however, there are two axis systems that we need to consider. One fixed, by us, in the laboratory and one fixed on the molecule itself. We have already seen how the **E**-**μ**-**v** vector correlation connects the two. In photofragmentation, many (effectively infinite) angular momentum states contribute to the outgoing wave packet whereas, in molecular photoionization, only a few orbital angular momentum partial waves contribute to the photoelectron wavefunction.

For the moment, we concentrate on photofragmentation. The anisotropy parameter can vary between 2 and −1, corresponding to the two limiting cases for the instantaneous fragmentation (axial recoil) of a diatomic molecule on a parallel or perpendicular transition respectively. In general the value of β will lie somewhere between these limits because of the finite dissociation time scale, and consequent smearing of the vector correlation function. Behaviour of this kind is often encountered with predissociation phenomena, where the dissociating molecule may require a number of vibrational periods before it can tunnel through the reaction barrier. In polyatomic molecules the value of β may also be reduced if the breaking bond does not lie along (or perpendicular to) the direction of the transition dipole moment. Combining these effects, one can show that, for a quasilinear molecule with moment of inertia I (Jonah 1971, Yang and Bersohn 1974),

$$\beta_{\text{eff}} = \frac{P_2(\cos\chi)}{2}\left(1 + 3\gamma\exp(\gamma)\int_{\gamma}^{\infty}\frac{\exp(-t)}{t}\mathrm{d}t\right), \tag{2}$$

where the parameter $\gamma = I/(8kT\tau^2)$ expresses the ratio of rotational period to the average dissociation time τ and χ is the angle between the parent molecule transition dipole moment and the fragment axial recoil velocity vector. So, by measuring the PAD in a photodissociation experiment, one learns about the symmetry and general 'landscape' of the electronically excited state and also the time scale (typically 50–5000 fs) of the dissociation.

These simple interpretive arguments rest on the assumption that the dynamics take place on a single potential energy surface (PES), in other words that the electronic and nuclear coordinates are decoupled within the framework of the Born–Oppenheimer approximation. This is rather like arguing that one can deduce the topography of a bobsleigh run on mist-shrouded mountain from the observation of

Figure 1. 'Winter Sports on Mt Fuji' after Hiroshige Ando. A straight fast trajectory is indicative of a steeply sloping but uncorrugated potential energy landscape or topography. Slaloming motion on the other hand is indicative of a steeply sloping valley in which the luge exhibits side-to-side motion such as in the 'spiral run' built for the Nagano 1998 winter Olympics. In the analogy, the molecule is vibrationally excited in this case.

the motion of the luge at the bottom of the run (figure 1). Thus, we might infer a highly twisting course from the observation of vibrational motion of the luge across the channel or a topography more resembling Mt Fuji from the observation of a high-speed linear trajectory.

This idea of a single adiabatic PES is at the heart of the London–Eyring–Polanyi–Sato model of elementary reactions on which much of our understanding of reaction mechanism is built (Polanyi 1987). Today, the interpretation of chemical dynamics for reactions which take place on a single surface is, largely, a solved problem (Simons 1999). Frequently, however, experimental observations cannot be so easily explained and it is increasingly becoming recognized that non-adiabatic transitions at potential energy curve (surface) crossings, for example, induced by vibronic coupling, can have an important influence on the product distributions in photodissociation and other similar dynamically controlled processes (Butler 1998). A well-known example is the 266 nm photolysis of methyl iodide. Long regarded as a prototypical example of a direct dissociation along a single reaction coordinate, methyl iodide was also the first molecular system to be studied by CPI (Chandler and Houston 1987). Close scrutiny of the available data reveals a complicated and interesting story.

The A-band photodissociation of methyl iodide is among the most widely studied dissociation process in a small polyatomic molecule (Johnson *et al.* 1996). In this system, the influence of the breakdown of the Born–Oppenheimer approximation appears in the population distribution between the iodine atom fine-structure levels.

The A-band absorption is dominated by a parallel transition to the $2A_1(^3Q_0)$ state that is adiabatically correlated to $I^*(^2P_{1/2})$. The contribution of a perpendicular transition to $3E(^1Q_1)$ correlating to $I(^2P_{3/2})$ is negligible. Nevertheless, a considerable amount of $I(^2P_{3/2})$ is formed (see for example Eppink and Parker (1999)), indicating the occurrence of a non-adiabatic transition from the $2A_1(^3Q_0)$ to $3E(^1Q_1)$ surface during the dissociation process. The $2A_1(^3Q_0)$ and $3E(^1Q_1)$ surfaces cross in C_{3v} symmetry but become avoided crossings by H_3C–I bending as the symmetry is lifted, forming a conical intersection (Amatatsu *et al.* 1996). Therefore, the vibronic coupling between the H_3C–I wag and C–I stretching modes plays an important role in the dissociation dynamics.

Another interesting example is the ultraviolet (UV) photodissociation of OCS. This is rather different from methyl iodide in that in OCS the same products, $CO(^1\Sigma^+) + S(^1D_2)$, are formed on each of the two coupled surfaces. Because of this the non-adiabatic coupling in OCS was not readily recognized. We have already mentioned that at short photodissociation wavelengths (157 nm) the CO product is vibrationally hot. By contrast, when OCS is excited into the first UV absorption band which peaks at around 220 nm, the CO product is found with negligible vibrational energy but considerable rotational energy (Sivakumar *et al.* 1988). It is tempting to interpret this observation in terms of the potential energy landscape. The first absorption band in OCS corresponds to absorption from the (linear) $^1\Sigma^+$ ground state to the $^1\Sigma^-$ and $^1\Delta$ states (Locker *et al.* 1983). These transitions are electric dipole forbidden; however, a bending deformation ($C_{\infty v} \rightarrow C_s$) will split the $^1\Delta$ state into A′ and A″ components and transform $^1\Sigma^-$ to A″ to which transitions from the ground state are weakly allowed. The expectation is that this bending motion will be transformed into rotational excitation when the molecule dissociates, and this is indeed the case. However, more interestingly, this rapid bending or 'internal rotation' of CO opens another non-adiabatic dissociation pathway, as described below.

Careful analysis shows the CO rotational distribution to be bimodal. This can be measured directly by vacuum ultraviolet (VUV) laser-induced fluorescence (LIF) of the CO fragment as Sivakumar *et al.* (1988), or indirectly by measurement of the translational energy release. The latter approach was adopted by Suzuki and co-workers (Katayanagi *et al.* 1995, Mo *et al.* 1996, Suzuki *et al.* 1998) who measured the speed and angular distribution of the $S(^1D_2)$ photofragments by CPI (see below). Figure 2 shows the translational energy distribution of the $S(^1D_2)$ atoms measured at 223, 235 and 248 nm from which it is clear that the corresponding CO rotational distribution must also be bimodal. This bimodality had been observed previously by Sivakumar *et al.* (1988) and by Sato *et al.* (1995b) but its origin was not clear.

The PAD of the S atoms observed by CPI, however, indicates that the low-energy S atoms are only formed in the direction parallel to the laser polarization, whereas the high-energy S atoms are formed in both the parallel and the perpendicular directions. This means that the bimodal distribution occurs only for dissociation from the $A'(^1\Delta)$ state and not from the $A''(^1\Sigma^-)$ state. *Ab initio* multireference configuration interaction calculations have been performed by Suzuki *et al.* (1998). Figures 3 and 4 show one-dimensional cuts of the calculated complete-active-space self-consistent field (CASSCF(9:10)) *ab initio* PESs along the interfragment co-ordinate R and the bending coordinate ϑ. It can be seen that in the linear configuration (figure 3) both the $^1\Delta$ and $^1\Sigma^-$ states are bound along R (below approximately 7 eV excitation energy) but that they are both crossed by a $^1\Pi$ state. It

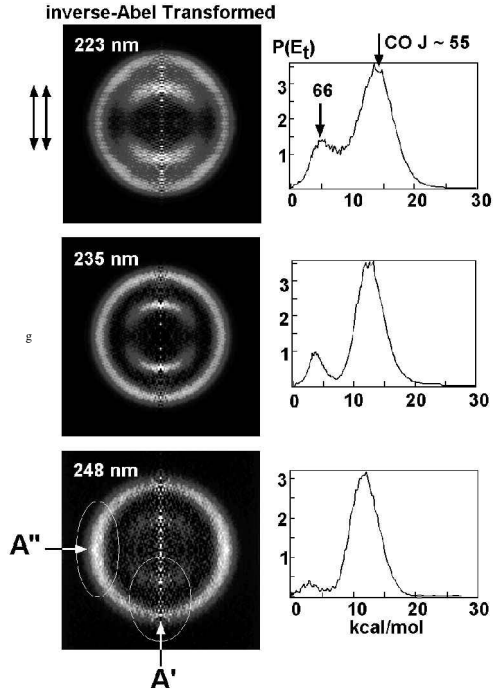

Figure 2. $S(^1D_2)$ Abel-transformed ion images and translational energy distributions observed from the photolysis of OCS at 223, 235 and 248 nm. It is clear that the translational energy distribution of the recoiling $S(^1D_2)$ atoms is bimodal. By considering the possible partitioning over the known vibrational and rotational levels, conservation of energy then dictates that the corresponding rotational energy distribution in the concomitant CO fragment is also bimodal. This effect can only be explained by non-adiabatic coupling between two PESs.

is this state that provides the adiabatic dissociation pathway as the molecule bends. Figure 4 shows that both the $A'(^1\Delta)$ and the $A''(^1\Sigma^-)$ state are strongly stabilized as the molecule bends. Therefore, the initial motion following excitation to either of these states is rapid bending. Close inspection of figure 4 also shows that both surfaces approach the ground-state surface at around $\vartheta = 65^\circ$ where the non-adiabatic transition from the $2A'(^1\Delta)$ to the $(1A''^1\Sigma^-)$ state might be anticipated. Detailed wave-packet calculations by Suzuki *et al.* (1998) have revealed that this is in fact the case and that this explains the observed bimodality in the CO rotational distribution.

Careful product state and angular distribution measurements, particularly if made at a number of excitation wavelengths, can therefore reveal and unravel non-Born–Oppenheimer dynamics. However, a more natural way to proceed is to attempt to probe the dynamics directly by mapping the time evolution of the initially prepared non-stationary state as it moves out towards the exit channel(s). To return to the winter sports analogy, our aim now is to follow the trajectory of the luge from the top of the mountain to the bottom, remembering that this is a quantum sleigh which might decide to take two paths simultaneously! The time scales are very short, a fraction of a picosecond, and it is only relatively recently that laser technology has developed to the point where these experiments are possible. The pioneering experiments of Zewail and co-workers paved the way (see Zewail (1997)).

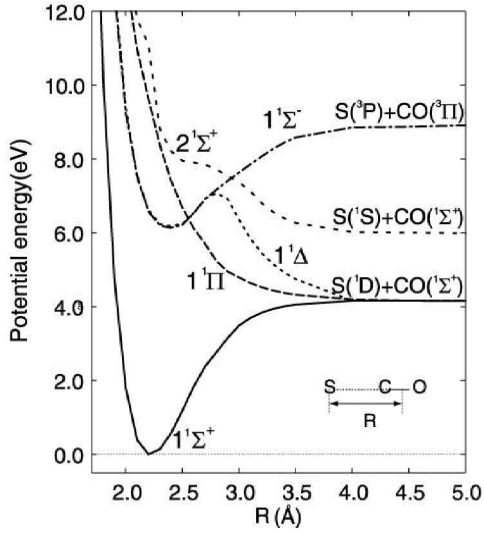

Figure 3. A cut through the lowest-energy calculated CASSCF(9:10) Born–Oppenheimer PESs (Jacobi or scattering coordinates) for OCS showing the radial dependence of the ground and excited states in the linear geometry with the CO distance $r = 1.13$ Å.

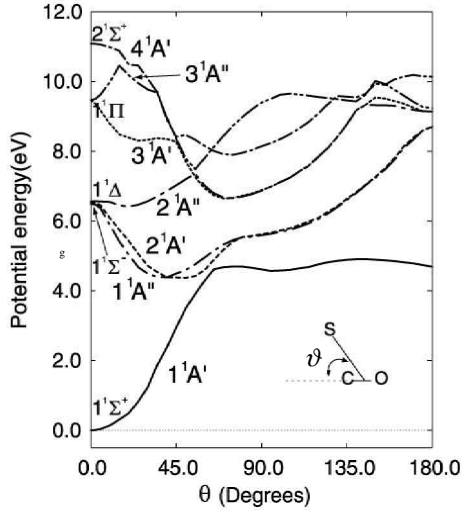

Figure 4. As figure 3 but showing angular dependence of the ground and excited states at a distance of $R = 2.2$ Å and $r = 1.13$ Å.

Our aim with this review article is to describe how the techniques of femtochemistry can be coupled with those of CPI to obtain time-resolved PADs. We shall show, particularly with respect to time-resolved photoelectron images, how non-adiabatic transitions (vibronic coupling) between PESs may then be distinguished from intramolecular vibrational redistribution (IVR) effects. We shall also discuss how pump–probe Coulomb explosion techniques may be coupled with imaging methods to provide a means of probing wave packets and PESs well away from the Franck–Condon region, providing us with, in effect, a molecular microscope capable of

capturing a nuclear wavefunction (Bandrauk *et al.* 1999). These two topics are complementary in that they approach the breakdown of the Born–Oppenheimer approximation from the opposite sides of the electronic and nuclear wavefunctions. Before embarking on this task we briefly review the current experimental state of the art in reaction dynamics and describe recent progress in the development of CPI.

2. Charged-particle imaging

Following the pioneering theoretical work of Polanyi, Wigner, Eyring and Evans in developing transition state theory, experimentalists began the task of verifying these ideas through observation. The project was demanding since the transition state is extremely short lived. The most direct confirmation of transition state theory has come from femtochemistry (Polanyi and Zewail 1995, Zewail 1996). Alternative approaches were transition state spectroscopy using negative ion photodetachment (Neumark 1992) and molecular-beam scattering experiments exploring dynamical resonances. The latter generally requires the measurement of rotationally resolved angular distributions for bimolecular collisions, which only became possible quite recently (Buntine *et al.* 1991, Suits *et al.* 1992, Bontuyan *et al.* 1993, Kitsopoulos *et al.* 1993, Schnieder *et al.* 1995, 1997, Yonekura *et al.* 1999, Lorenz *et al.* 2000).

From the 1960s to the late 1980s, crossed molecular beam methods employing a rotatable quadrupole mass spectrometry detector provided the most detailed data on polyatomic reaction dynamics (Casavecchia 2000). This fact was recognized by the award of 1986 Nobel prize for Chemistry to Herschbach, Lee and Polanyi for their contributions concerning the dynamics of chemical elementary processes and who had pioneered molecular-beam and chemiluminesencent methods. Laser-based detection methods were less commonly used in the early days because of the difficulties associated with generating tunable UV radiation, but by the mid-1980s *Q*-switched laser technology, coupled with nonlinear frequency-mixing techniques, had advanced to a stage where laser ionization schemes through resonance enhanced multiphoton ionization (REMPI) were commonly applied (Belbruno 1995). Although it is not a universal detection technique, the advantage of a REMPI scheme is that the product species can be ionized and so efficiently detected, *state selectively*. Quantum state selectivity is achieved because the first photon(s) absorbed must excite a stable state in the molecule or atom (figure 5). By contrast, a conventional molecular beam machine fitted with mass spectrometry detection relies on time of flight (TOF) alone to deduce the internal energy distribution; so it is extremely hard to achieve rotational resolution of the product distribution even for a triatomic reaction $A + BC \rightarrow AB + C$ and impossible for tetratomic systems $AB + CD \rightarrow AC + BD$ and larger using this technique. Chandler and Houston (1987) realized that REMPI state selection could be coupled to a two-dimensional (2D) ion detector to obtain both the speed and the angular distribution of the products in an experimental apparatus with no moving parts. This also makes crossed molecular beam apparatus easier to build (although the experiments are not necessarily much easier to perform!).

The first champions christened the new technique photofragment or ion imaging (Chandler and Houston 1987, Chandler *et al.* 1989, 1990) but it has since come to be known as velocity map imaging (VMI), as a result of relatively recent improvements in the design of the charged-particle 'optics' employed (Eppink and Parker 1997). Because we also want to incorporate Coulomb explosion imaging (CEI) and

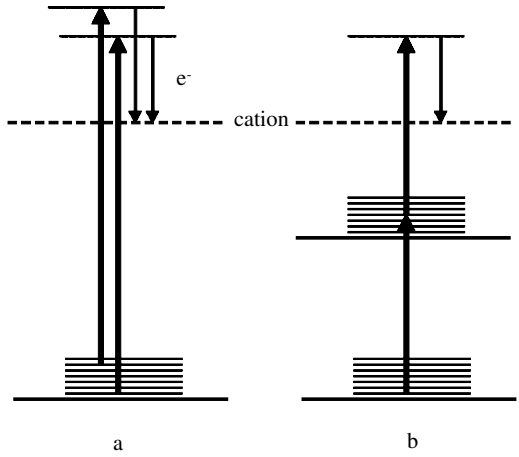

Figure 5. (*a*) One-photon ionization and (*b*) $(1+1)$ REMPI. The former ionizes all molecules in any populated quantum state while REMPI ionizes only an ensemble of molecules in the quantum state connected to the intermediate state by absorption of the first photon.

photoelectron imaging into our discussions we prefer to refer to CPI. The basic idea behind CPI has been reviewed by a number of workers (Thoman *et al.* 1988, Whitaker 1993, Heck and Chandler 1995, Houston 1995, Heck 1997); so we shall not dwell on it here. Briefly, anisotropic velocity distributions of charged particles are characterized by projecting the charged species on to an imaging detector in a TOF mass spectrometer. In the earliest imaging machines the TOF mass spectrometer was based on the classic Wiley–McLaren (1955) design in which transmissive wire mesh grids are used to generate a uniform electric field across the axis of the flight tube. CPI instruments now generally employ an immersion lens to extract the ions into the TOF region (Chandler and Parker 1999).

The particle detector at the end of the field-free TOF region consists of a microchannel plate (MCP) or microsphere plate (MSP) backed by a phosphor screen. For reasons of spatial resolution, MCPs are generally preferred over MSPs, although the latter are cheaper and more robust. When a charged particle enters one of the channels (about 10 μm in diameter), in the MCP, secondary electrons are emitted. These are amplified in the channel and accelerated towards the phosphor screen. The electron impact on the phosphor produces a bright light spot that indicates the arrival position of a charged particle (ion or electron) on the MCP. The image on the phosphor screen is captured by the charged-coupled device (CCD) camera and integrated for a number of laser shots. The velocity components of the detected particles parallel to the detector face (v_x, v_y) are readily determined from the flight time t and the arrival positions $(x, y)_i$ from the relation $v_x = x/t$ and $v_y = y/t$. In an actual experiment, some background ions may be formed by the pump and probe lasers, but ions with different masses can be discriminated by their flight times from the ionization region to the detector; the flight times of ions are roughly proportional to $m^{1/2}$. Thus, an ion image can be selectively observed for a particular mass of interest by time gating either the MCP or the camera.

CPI generally uses REMPI to detect the atoms and molecules in a particular quantum state (see figure 5). Therefore, the observed image provides the scattering

distribution of state-selected products. It should be noted that electron impact, one-photon, or non-resonant multiphoton ionization methods cannot provide such state selectivity. Furthermore, the time resolution of a TOF measurement is generally not sufficient to resolve more than the vibrational energy distribution in a molecular co-product. An exception to this statement is the Rydberg tagging technique (Schnieder *et al.* 1997, Cook *et al.* 2000). Here fragments are first 'tagged' by exciting them to a very high Rydberg state. Angular momentum mixing causes these states to have very long radiative lifetimes (Chupka 1993) and so the excited atomic or molecular fragment can fly from the interaction region to a detector tens of centimetres away. Here they are field ionized by passing close to a charged mesh and the resulting ions easily detected. The method has the advantage over CPI that the tagged atoms, although highly excited, are charge neutral and so do not interact with each other, which obviates the space-charge problems observed in CPI if too many products are ionized. On the other hand, Rydberg tagging is practically limited to studies in which H or D atoms are produced since light species give the best kinetic energy resolution. However, see the papers by Drabbels *et al.* (1995) and Morgan *et al.* (1996) in which CO from ketene photolysis was detected by excitation to a metastable triplet state.

As described above, in the 2D imaging apparatus developed by Chandler and Houston (1987) a uniform accelerating electric field was formed using wire meshes. However, with this design the ions are slightly deflected by field distortion near the wires. In addition, the observed ion image is the convolution of the recoil velocity distribution of the ions and the volume defined by the ionizing laser beam profile as it crosses the molecular beam. These two problems limited the imaging resolution. It may be recalled, however, that the one-dimensional (1D) Wiley–McLaren TOF mass spectrometer was designed to eliminate the effects of a finite ionization volume along the flight axis by introducing 'space focusing'. Likewise, '2D space focusing' perpendicular to the TOF axis can be used to eliminate the blurring of an ion image due to the finite interaction region between the ionizing laser and the molecular beam. Electrostatic focusing in this way has the effect of mapping ions created in different locations in the interaction volume, but with the same velocity, to the same spot on the MCP detector, giving rise to the name VMI. Eppink and Parker (1997) showed that such a focusing effect is obtained simply by removing the wire meshes from the acceleration electrodes to create an immersion lens. This new design also improves the ion transmission through the flight tube, which had previously been limited to 60–90% for each mesh used. On the other hand, the electrostatic lens effect of the VMI design magnifies the ion image, and the magnification factor needs to be determined accurately in a separate calibration experiment to obtain v_x and v_y correctly. The mass resolution is not as good as a Wiley–MacLaren TOF mass spectrometer but this does not normally present any problems in imaging applications. A standard immersion lens is astigmatic; so the velocity resolution across the face of the detector is not quite uniform. However, Wrede *et al.* (2000) have assessed these effects and find that with careful design of the ion optics the degree of astigmatism is similar to the combined resolution limit of the MCP plates, camera pixel size and velocity spread in the parent molecular beam.

The final improvement made to the CPI experiment has been the introduction of 'event counting'. Even well made MCPs or MSPs rarely have a uniform response across their entire surface. Furthermore, the sensitivity of the detector surface changes with use. This introduces variations in the brightness of the image across the detector. However, whatever their relative intensity, one knows that the bright

spots, which are recorded by the CCD camera, represent the arrival of *individual* ions. It is nowadays quite straightforward to perform image processing on each CCD frame to locate the centre of gravity of each spot and simply to count it. Three reports describing slightly different approaches to event counting emerged independently at roughly the same time (Chang *et al.* 1998, Cooper *et al.* 1998, Yonekura *et al.* 1999) and it is now quite commonly applied.

A velocity map is a projection of the three-dimensional (3D) fragment velocity distribution on to a 2D detector plane. Therefore, the data must be numerically inverted to recover the original 3D distribution for quantitative analysis. It can be shown, mathematically, that a cylindrically symmetric 3D object can be reconstructed from a single projection image if the projection plane includes the symmetry axis. The most commonly employed inversion method is the Abel–Hankel transform (see for example Whitaker (2000)), but other methods such as back projection (Budinger and Gullberg 1974, Sato *et al.* 1995a) and onion peeling are also used (Winterhalter *et al.* 1999).

In a photodissociation experiment, the flux of photofragments created by the pump laser is cylindrically symmetric around the polarization vector. However, when the fragments are turned into ions by the probe laser this symmetry can be broken, making the inverse Abel transform inapplicable (Suits *et al.* 1993, Blunt and Suits 1997). This is because the ionization efficiency varies with the relative angle between the polarization vector of probe laser and the angular momentum of the fragments if the angular momentum is polarized (Mo *et al.* 1996, 1999, Ahmed *et al.* 1999). Such angular momentum polarization can occur in molecular products (the so-called **v**–**J** correlation) because of mechanical torque imparted during dissociation (Hall and Houston 1989) or, in atomic fragments, by conservation of electronic angular momentum (Van Brunt and Zare 1968). When the pump and probe laser polarizations are set parallel to each other cylindrical symmetry is always ensured, irrespective of angular momentum polarization. Therefore, this polarization set-up and a projection direction perpendicular to the symmetry axis are usually employed in ion imaging. Note, however, that, although this configuration forces the data to be Abel invertible, the extracted distribution must be corrected for alignment effects to obtain the true photofragment velocity distribution. The treatment of this polarization effect and its application to the extraction of useful information concerning reaction stereodynamics has been discussed quite extensively (see for example Glass-Maujean and Beswick (1989), Kupriyanov and Vasyutinskii (1993), Siebbeles *et al.* (1994), Mo and Suzuki (1998), Bracker *et al.* (1999), Rakitzis and Zare (1999) and Underwood and Powis (2000)). In particular, atomic orbital orientation has been discussed recently in terms of quantum interference effects (Siebbeles *et al.* 1994, Rakitzis *et al.* 1999a, b, Kim *et al.* 1999), which are analogous to electron spin polarization effects in photoionization (see for example Cherepkov (1983)). In inelastic and reactive scattering imaging experiments it is usual to image perpendicularly to the plane defined by the two velocity vectors of the collision partners (Suits *et al.* 1992, Bontuyan *et al.* 1993, Yonekura *et al.* 1999, Lorenz *et al.* 2000) (see also Kitsopoulos *et al.* (1993)). For other recent work in this area, such as experimental observations of dynamical resonance in reactive scattering, see also Fernández-Alonso *et al.* (2000) and Kendrick *et al.* (2000), Liu *et al.* (2000) and Skodje *et al.* (2000).

There are other 2D position-sensitive detectors, such as the wedge-and-strip anode detector, in which the arrival position of a charged particle is calculated

electronically, and which are used in some CPI applications. While a camera-based system can detect the arrival of many particles at once, most electronic 2D detectors have a dead time of about 1–10 ns after the arrival of a single charged particle. This makes them unsuitable for the type of CPI experiment described by Chandler and Houston (1987), where typically 10–100 ions arrive at the detector in less than 30 ns. On the other hand, a disadvantage of a CCD-based detector is that it has a poor timing resolution. Although double-shot exposure by electronic masking of the CCD chip can be achieved and an interframe time resolution of less than 100 ps has been reported (Amitay and Zajfman 1997), electronic imaging detectors have much superior time resolution and duty cycle (Brenot and Durup-Ferguson 1992). Simultaneous measurements of both the arrival position (x, y) and the arrival time t of the charged particles are essential for photoelectron–photoion coincidence (PEPICO) experiments and also for some CEI experiments, as described below. A new class of complementary metal–oxide–semiconductor (CMOS) optical detectors have reportedly reached frame rates of $1000\,s^{-1}$; so it may become possible to perform coincidence experiments with optical position sensitive detectors in the future.

3. Time-resolved photoelectron imaging

Over the past 20 years or so, advances in laser technology, particularly the discovery of self-mode locking in Ti:sapphire (see for example Reid and Wynne (2000)), have opened an exciting new era of femtochemistry where physical chemists can witness the breaking and forming of chemical bonds in 'real time'. Although not the first demonstration of real-time transition state spectroscopy or 'stroboscopy' (Zewail 2000), a landmark achievement in this area was the observation by pump–probe LIF spectroscopy of the dissociation of NaI (Rose *et al.* 1988, 1989, Rosker *et al.* 1988). The curve crossing of the ionic ground state Na^+I^- with the covalent excited state NaI, correlating to $Na(^2S_{1/2}) + I(^2P_{3/2})$, has long been recognized as a non-adiabatic transition. Taking this classic example, Rose *et al.* (1988) launched a wave packet on the excited state ($^1\Sigma_0^+$) by photoexcitation, with a femtosecond pump pulse, from the ground state and observed the subsequent dynamics by LIF using a series of time delayed femtosecond probe pulses. The number of Na product atoms, probed at the D line, exhibited a stepwise increase as a function of time delay. This signal is the result of non-adiabatic tunnelling of the wave packet to the ground state potential each time that it encounters the curve-crossing region as it oscillates back and forth on the excited-state PES. Likewise LIF observed following excitation into the red wing of the D line showed a corresponding decrease as the oscillating wave packet on the excited-state surface is depleted (figure 6).

Following this ground-breaking work, Engel and Metiu proposed an elegant pump–probe experiment on NaI. Engel and Metiu (1989a, b) predicted that photoionization from the excited state surface should produce different products depending on whether the wave packet was close to the inner or outer turning points at the instant of ionization. Around the outer turning point, they argued that photoionization should produce Na^+ ions, while NaI^+ ions should be produced around the inner turning point. Later Braun *et al.* (1996) calculated the photoelectron energy spectra expected for such a pump–probe photoionization experiment. The proposal by Engel and Metiu was experimentally tested much later by Jouvet *et al.* (1997).

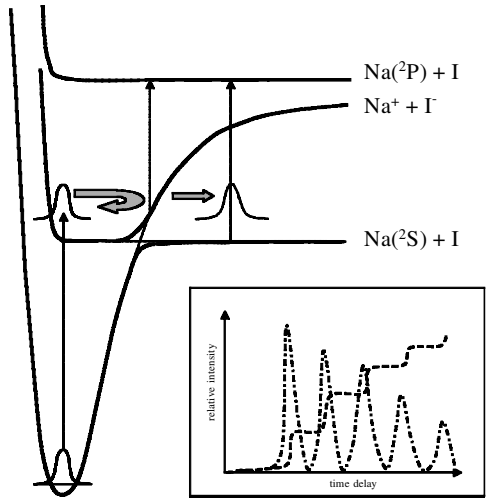

Figure 6. A schematic diagram illustrating the principle of the experiment performed by Rosker *et al.* (1988). A vibrational wave packet is created on the first excited state of NaI by the coherent excitation of a number of vibrational states using a femtosecond pulse. The time evolution of the wave packet is monitored by a second time-delayed femtosecond laser pulse. If the wavelength of the probe pulse is tuned into resonance with the Na D line, the fluorescence signal from $Na(^2P)$ builds up as shown by the broken curve in the inset as more and more Na atoms are created each time that the wave packet encounters the crossing point. If the probe laser is tuned slightly off resonance, the signal exhibits oscillations as shown by the chain curve in the inset each time that the wave packet enters the 'Franck–Condon window' connecting the NaI* potential energy curve to the second excited state curve correlating to $Na(^2P) + I$.

The use of photoionization as a probe of the excited state dynamics has advantages compared with LIF since ionization can occur from any part of the potential for a sufficiently high-energy photon. The photoabsorption wavelength required to excite a bound–bound transition in a LIF experiment is a function of nuclear coordinates, so the probe laser frequency needs to be scanned in order to observe the entire region of the PES. Because of the bound–free nature of ionization, on the other hand, the photoelectrons can carry away the energy difference between the different vibrational levels of the cationic state:

$$E_e = \hbar(\omega_1 + \omega_2) - IP_0 - E_v^+, \tag{3}$$

where E_e is a photoelectron kinetic energy, IP_0 is the adiabatic ionization potential, E_v^+ is the vibrational energy of the cation, and ω_1 and ω_2 are the angular frequencies of the pump and probe laser fields respectively. This means that the resonance condition can be fulfilled for ionization of a wave packet to a range of vibrational levels in the cationic state with a ***fixed laser frequency***.

In an ideal situation, the photoelectron kinetic energy distribution is determined by the Franck–Condon factors between the vibrational wave packet in the neutral excited state $|\psi(t)\rangle$ and the vibrational wavefunctions in the cationic state $\langle\chi_v^+|$:

$$P(E_e) \propto \sum_{\mathbf{v}} |\langle\chi_{\mathbf{v}}^+|\psi(t)\rangle|^2. \tag{4}$$

However, there is another factor to consider, as the results obtained by Jouvet *et al.* (1997) for the femtosectond pump–probe photoionization of NaI demonstrated. They found that, although the observed Na^+ signal was in good agreement with the theoretical predictions made nearly 10 years earlier by Engel and Metiu (1989a, b), the NaI^+ signal also arose from ionization close to the outer turning point. This was at odds with the prediction. It turns out that the $NaI \rightarrow NaI^+$ cross-section from the outer turning point is much larger than that from the inner turning point. At the outer turning point on the excited state potential the bonding is essentially ionic and photoionization effectively corresponds to ionization of I^- (with a 20 Mb cross-section for a photon energy of 4–5 eV). At the inner turning point, by contrast, the bonding is essentially covalent and the process is essentially photoionization of Na (with a cross-section of the order of 0.1 Mb). Thus, the large ionization efficiency at the outer turning point produces a substantial NaI^+ signal. Engel and Metiu (1989a, b) had assumed, incorrectly, a uniform ionization cross-section at all interatomic distances, which led them to overestimate ionization from the covalent part of the excited state potential. Charron and Suzor-Weiner (1998) used an empirical form of the ionization cross-sections from the covalent and ionic parts of an excited state potential to simulate the observations by Jouvet *et al.* (1997) and obtained good agreement with the experimental observations.

Although the value of the pioneering work by Engel and Metiu is undiminished by this subtle deficiency, the example clearly illustrates the importance of an accurate evaluation of the ionization cross-section, especially when the electronic character of the probed state changes dramatically as a function of nuclear geometry. The work by Jouvet *et al.* showed that the observation of the wave-packet dynamics of NaI on the covalent part of the potential is impractical owing to the small photoionization cross-section. More recent work on the dynamics of the $^1\Sigma_u^+(1)$ double-minimum state in Na_2 by Arasaki *et al.* (2000) considered the ionization cross section from different regions of the potential energy curve accurately, and in this case the excited-state wave-packet dynamics can be followed by time-resolved photoionization.

The dependence of the photoinization cross-section on the electronic character of the PES can be turned to advantage since it opens a way for us to observe the time-dependent electron configuration (or configuration interaction) during the course of a chemical reaction (Blanchet *et al.* 1999). Such information is essential to the understanding of non-adiabatic dynamics, where the electronic character changes rapidly in the curve (surface) crossing region.

In seminal work on femtosecond time-resolved photoelectron spectroscopy, Seel and Domcke (1991) considered photoionization of the $S_1(n, \pi^*)$ and $S_2(\pi, \pi^*)$ states of pyrazine to the cationic states $I_0(n^{-1})$ and $I_1(\pi^{-1})$. They examined two cases: case (*a*) in which S_1 and S_2 are ionized to I_0 and I_1 respectively, and case (*b*) where both S_1 and S_2 are ionized to I_0. Since the $S_2(\pi, \pi^*) \rightarrow S_1(n, \pi^*)$ internal conversion is extremely fast, $\tau = 30$ fs, their theoretical prediction has yet to be fully investigated experimentally (Stert *et al.* 2000), but their work clearly expresses the basic idea of using two cationic electronic states as templates for probing electron dynamics in molecules such as pyrazine.

The time dependence of the photoelectron energy distribution, therefore, is likely to be a rich source of information for understanding excited-state dynamics. This concept dates back to, at least, the mid-1980s, with observations of intersystem crossing in triazine (Pallix and Colson 1985) and benzene (Sekreta and Reilly 1988) by nanosecond time-resolved photoelectron spectroscopy. Time-resolved zero-

kinetic-energy spectroscopies have also been successful in this regard and interested readers should refer to other excellent review articles (see for example Powis *et al.* (1995), and particularly the article by Knee (1995) and references therein).

We have already alluded to the idea that the photoelectron angular distribution (PAD) is another important source of information to be utilized. Note that we use the same acronym to stand for both photoproduct and photoelectron angular distribution; it should generally be clear from the context whether we are referring to molecular or atomic products or to photoelectrons. In the laboratory frame, the PAD is a measure of the flux of outgoing photoelectrons measured as a function of angle ϑ with respect to the ionization laser symmetry axis (the electric vector in linearly polarized light). For one-photon ionization, the definite spin and parity of the ionizing photon defines the PAD observable for a randomly oriented ensemble of molecular targets (Yang 1948):

$$\frac{\mathrm{d}\sigma}{\mathrm{d}\Omega} = \sum_{K=0,2} A_K P_K(\cos\vartheta) = \frac{\sigma}{4\pi}[1 + \beta P_2(\cos\vartheta)]. \tag{5}$$

Here, $P_K(\cos\vartheta)$ is a Legendre polynomial and the A_K are coefficients describing the weighting of the Kth moment to the differential cross-section. For a two-photon process, such as $(1+1')$ REMPI, the pump pulse creates a partial molecular alignment in the intermediate level, and this introduces a higher moment in the PAD. When the pump and probe laser polarizations are parallel to each other the PAD becomes

$$\frac{\mathrm{d}\sigma}{\mathrm{d}\Omega} = \frac{\sigma}{4\pi}[1 + \beta_2 P_2(\cos\vartheta) + \beta_4 P_4(\cos\vartheta)]. \tag{6}$$

The physical interpretation of the laboratory-fixed PAD is particularly clear for the case of one-photon ionization of a one-electron atom. According to Bethe (1933) and Cooper and Zare (1968) the anisotropy parameter is given by

$$\beta = \frac{l(l-1)r_{l-1}^2 + (l+1)(l+2)r_{l+1}^2 - 6l(l+1)r_{l+1}r_{l-1}\cos(\eta_{l+1} - \eta_{l-1})}{(2l+1)\left[lr_{l-1}^2 + (l+1)r_{l+1}^2\right]}, \tag{7}$$

where $r_{l\pm1}$ are the transition dipole matrix elements for the $l \pm 1$ components of outgoing photoelectron wavefunctions, and $\eta_{l\pm1}$ denote the phases of these waves. For an s electron, $l = 0$, the outgoing photoelectron is a pure p wave, yielding $\beta = 2$. For other initial electron orbital angular momentum states, the magnitude of the anisotropy parameter is reduced as a result of interference between the two outgoing partial waves that are now possible (through the $\Delta l = \pm 1$ electric dipole selection rule).

In the case of an atom, there is no body-fixed axis to refer to. However, a molecule has its own body-fixed frame that is tilted from the space-fixed (or laboratory) frame by Euler angles (θ, ϕ, χ).The distribution of the molecular axes in the space-fixed frame can be expressed by

$$F(\theta, \phi) = \sum_{KQ} A_{KQ} Y_{KQ}(\theta, \phi), \tag{8}$$

where K and Q are the rank and order respectively of the axis distribution, and the Y_{KQ} are spherical harmonics. In a cylindrically symmetric system, the terms with $Q \neq 0$ are all zero. In a pump–probe experiment on an initially randomly oriented

molecular ensemble, photoabsorption of the pump pulse creates an anisotropic distribution of excited-state molecules. The orientation and alignment of the molecular axes in the excited state ensemble can be described by a superposition of spherical tensors with the highest rank $K = 2n$, where n is the number of photons absorbed in the excitation step. The PAD in the space-fixed frame is then expressed (Reid and Underwood 2000) as

$$\frac{\mathrm{d}\sigma}{\mathrm{d}\Omega} = \int \sum_{KQ} A_{KQ}\, Y_{KQ}(\theta, \phi) \left| \langle \hat{\mathbf{k}}, r^{-}; \eta_{+} | \mathbf{d} \cdot \hat{\mathbf{e}} | \eta \rangle \right|^2 \sin\theta \, \mathrm{d}\theta \, \mathrm{d}\phi \, \mathrm{d}\chi, \tag{9}$$

where $\langle \hat{\mathbf{k}}, r^{-}; \eta_{+}|$ is the composite wavefunction of the outgoing photoelectron defined by the direction $\hat{\mathbf{k}}$ and the set of quantum numbers characterizing the ion core, η_{+}, the ket $|\eta\rangle$ represents the vibronic wavefunction of a neutral excited state, $\mathbf{d}$ is a transition dipole moment and $\hat{\mathbf{e}}$ is the electric vector of light. The above formula can be recast in the form

$$\frac{\mathrm{d}\sigma}{\mathrm{d}\Omega} = \sum_{LQ} \beta_{LQ}\, Y_{LQ}(\theta_k, \phi_k), \tag{10}$$

with

$$\beta_{LQ} = \sum_{K} A_{K-Q} P_{KLQ}, \tag{11}$$

where L runs from zero up to $K_{\max} + 2$. The analogous expression to equation (7) for β_{LQ} can be found in the paper by Underwood and Reid (2000), but we just need to note that the functions P_{KLQ} involve cross-terms of the dipole transition matrix elements inducing interference, as in the case of a one-electron atom. Clearly, the PAD changes when the vibronic character of $|\eta\rangle$ varies as the result of intramolecular electronic dephasing (or non-adiabatic transition).

Another source of the modulation of the PAD is the alignment parameter A_{K-Q}. When a short pulse creates a coherent superposition of rotational states, forming a rotational wave packet, the alignment parameter A_{K-Q} varies as a function of time, resulting in characteristic time revivals of the alignment. Felker and Zewail (1987) pioneered the use of LIF to observe these revivals (see also Baskin *et al.* (1987)) and to establish rotational coherence spectroscopy (RCS) as a tool for determining molecular structure (RCS provides information on the rotational level structure of large molecules that are often difficult to study in the frequency domain). In principle, the PAD should also manifest these revivals, as discussed by Seideman (1997) and Althorpe and Seideman (1999) for IVR and by Reid *et al.* (1999) for Coriolis coupling. A clear example of rotational coherence will be presented in a later section of this article for pyrazine.

If the molecules have a definite orientation in space, the PAD can be expressed as

$$\frac{\mathrm{d}\sigma}{\mathrm{d}\Omega} = \sum_{K=0}^{2l_{\max}} A_{KM}\, Y_{KM}(\theta, \phi), \tag{12}$$

where θ and ϕ are measured from the Z axis in the molecular frame, and $l_{\max}$ is the largest orbital angular momentum component of the outgoing photoelectron (Dill 1976, Dill *et al.* 1976). The coefficients A_{KM} include quantities such as the transition dipole matrix elements and the phase shifts of electron partial waves (Chandra and Chakraborty 1991). The PAD measured in the molecular frame provides far richer

information on the ionization dynamics than the PAD measured in the laboratory frame. This is because the ensemble averaging over all possible molecular orientations is then avoided.

Kaesdorf *et al.* (1985) oriented gaseous CH_3I using a hexapole state selector and measured the photoelectrons generated by VUV light in the direction parallel and antiparallel to the orientation field. They observed asymmetry in the photoelectron angular distribution that showed that ejection from the iodine end of the molecule was favoured, which, although an unsurprising result, gives confidence that one can control the molecular orientation and alignment sufficiently to measure PADs in the molecular frame. Golovin (1991), Golovin and Cheremnykh (1991) and Hatherly *et al.* (1995) have employed an angle-resolved photoelectron–photoion coincidence (ARPEPICO) technique in conjunction with dissociative ionization to measure the PAD for molecules fixed in space. When the molecule is dissociatively ionized, a photoelectron is ejected and then the molecular ion core breaks apart. If the ion dissociates within its rotational period, the fragments are, if it is a two-body dissociation, ejected along the molecular axis. One can then measure the angular correlation between the recoil velocity of the ion and the electron. Thus, the electron PAD can be measured with respect to the fragment recoil velocity direction (which is equivalent to the molecular axis) even though the molecules are initially randomly oriented.

Note, however, that the coincidence technique is only applicable to 'dissociative' ionization. Furthermore, the method may not be useful for obtaining the PAD in the molecular frame for large molecules that decompose with finite lifetimes after molecular rotation. An alternative approach to obtain the PAD in the molecular frame is to measure the PAD in the laboratory frame for an ensemble of aligned or oriented molecules. Previously, Leahy *et al.* (1992) and Wang and McKoy (1995) studied the photoelectron angular distributions for $(1 + 1')$ photoionization of NO molecules in the $A\,^2\Sigma$ state. This is, essentially, the measurement of the PAD for NO aligned by a pump laser. Similarly, as we shall shortly discuss, one can use the same idea to interpret time-dependent PADs measured by ultrafast pump–probe photoelectron imaging.

The photoionization quantum yield is usually small close to the ionization threshold because there is often a high density of super-excited neutral states that carry oscillator strength in this region. In most theoretical treatments of time-resolved photoelectron spectroscopy, the outgoing electrons are assumed to be unscattered by other valence electrons, so reducing the photoionization process to the projection of the neutral wave packet on to the cationic state wavefunctions. In reality, the interactions between the ionization continuum and super-excited neutral states cannot be completely excluded, but this subtlety has not been fully examined so far.

Pulsed-field ionization (PFI) zero-kinetic-energy photoelectron spectroscopy provides an extremely high-resolution photoionization spectrum that mimics a photoelectron spectrum (Müller-Dethlefs and Schlag 1991). The method detects resonances with high Rydberg states converging to each rovibronic state of a cation by scanning the laser frequency, but *not* the photoelectrons with positive energies. In the femtosecond regime, the high spectral resolution obtainable with PFI zero-kinetic-energy photoelectron spectroscopy is severely limited by the uncertainty principle, and other methods, which provide the entire photoelectron speed and

angular distribution with a fixed ionization laser frequency, become much more advantageous.

In photoelectron spectroscopy the kinetic energy of the ejected electrons can be measured in a number of ways, such as with an electrostatic energy analyser by the TOF technique (Rinnen *et al.* 1989). For (pseudo)continuous light sources, electrostatic analysers have been widely utilized, while most pulsed-laser experiments employ a TOF method. The small acceptance angle of TOF electron spectrometers was much improved by invention of the magnetic bottle spectrometer by Kruit and Read (1983). On the other hand, the angular resolution is sacrificed in a magnetic bottle spectrometer.

The advantage of a photoelectron imaging (PEI) spectrometer is that all the photoelectrons are perfectly collected by an electric field, making the method extremely sensitive and efficient. The detection efficiency is only limited by the quantum yield of the MCP detector, which is about 60%. Since PEI measures photoelectrons with different wave-vectors simultaneously, it provides reliable measurements of both speed and angular distributions in a single experimental configuration. In PEI, the photoelectrons are accelerated in order to make the whole electron cloud smaller than the diameter of the position-sensitive detector. Because of the high kinetic energies thus imparted to the photoelectrons, they are almost insensitive to stray fields in and around the apparatus. This is in sharp contrast with the great care that needs to be taken about contact potentials and the terrestrial magnetic field in conventional photoelectron spectroscopy. With velocity mapping and real-time image processing such as event counting, the photoelectron energy resolution reaches the instrumental limit given by the number of pixels in the CCD camera (Chandler and Parker 1999). For a 400×400 pixel camera, the energy resolution for the fastest electron is about $\Delta E = 10\,\text{meV}$ at $E = 1\,\text{eV}$. This is more than sufficient for femtosecond pump–probe experiments. PEI provides uniform sensitivity for photoelectron energies down to extremely slow electrons ($E_{\text{kin}} < 0.2\,\text{eV}$). This is in marked contrast with magnetic bottle spectrometers which are relatively insensitive to slow photoelectrons.

2D PEI was first applied to the ionization of Xe by Helm *et al.* (1993) and Saeed *et al.* (1994). They observed ionization branching into the $^2P_{3/2}$ and $^2P_{1/2}$ states of Xe^+ and applied multichannel quantum defect theory to find the influence of the Cooper minimum in the $ns \rightarrow \varepsilon p$ transition amplitudes on the ionization dynamics (see also Bordas *et al.* (1994, 1995)). The ionization dynamics of iodine atoms has also been studied using PEI by Kang *et al.* (1995) and Jung *et al.* (1997). When the photoelectron kinetic energy E_{kin} is much smaller than the acceleration energy U, reconstruction of the 3D scattering distribution from the 2D projection is straightforward. Special cases when the ratio $\rho = U/E_{\text{kin}}$ is small have been discussed, and a general reconstruction algorithm has been presented by Bordas *et al.* (1996) and Winterhalter *et al.* (1999). Bordas (1998) and Bordas and Pinare (1998) have also examined the secondary interactions of slow photoelectrons with the residual ion core. Pinare *et al.* (1998, 1999) have examined photoemission from tungsten clusters by utilizing the sensitivity of PEI to slow photoelectrons. Slow PEI experiments on Xe atoms have also recently been reported by Nicole *et al.* (2000).

The 2D PEI detector described above is based on an MCP and a CCD camera. As discussed above, there are also electronic 2D position-sensitive detectors that calculate the arrival position of charged particles electronically. Because of their excellent time resolution, these detectors are particularly suitable for PEPICO

experiments. The earliest measurements of molecular frame PADs were performed by line-of-sight detection of both ions and electrons, which yielded extremely low count rates. Since the mid-1990s, 2D position-sensitive detection of ions (Golovin 1998) and 1D multiplex detection of electrons (Downie *et al.* 1995, Downie and Powis 1999a, b) have made ARPEPICO experiments more feasible. More recently, Davies *et al.* (1999) and Takahashi *et al.* (2000) have developed ARPEPICO spectrometers with complete detection of ions and electrons for all solid angles.

3.1. *Examples of time-resolved photoelectron imaging: the S_1 state of pyrazine*

Since the pioneering work by Frad *et al.* (1974) and Lahmani *et al.* (1974), the $S_1(^1B_{3u})$ state of pyrazine has been the best-known example of an intermediate case in molecular radiationless transition theory. It was predicted (Bixon and Jortner 1968, Avouris *et al.* 1977) that coherent excitation of an intermediate case molecule should exhibit biexponential fluorescence decay $I(t)$:

$$I(t) \propto |\langle s|\psi(t)\rangle|^2 = \sum_{n\neq m}\sum A_n A_m^* \alpha_n \alpha_m^* \exp\left[-\mathrm{i}(\varepsilon_n - \varepsilon_m)t\right] \exp\left(\frac{\gamma_n + \gamma_m}{2} t\right) + \sum_n |A_n|^2 |\alpha_n|^2 \exp\left(-\gamma_n t\right), \tag{13}$$

where the fast decay is due to the ultrafast dephasing of the optically prepared singlet state $|s\rangle$ into a state of mixed singlet–triplet character (the first term of the above formula) and the slow decay is the depopulation of this mixed state (the second term). For definitions of the terms appearing in equation (13) see equation (II.10) in the paper by Lahmani *et al.* (1974). The biexponential fluorescence decay of S_1 pyrazine was extensively studied in the 1980s, and a lengthy debate ensued as to whether the fast component experimentally observed was due to the predicted dephasing or Rayleigh–Raman scattering (McDonald *et al.* 1981, Okajima *et al.* 1982, Yamazaki *et al.* 1983, Knee *et al.* 1985, Lorincz *et al.* 1985). With the development of picosecond laser spectroscopy, convincing evidence for dephasing ($\tau \approx 110$ ps) was obtained, and consistency was found with molecular eigenstate spectroscopy pioneered by van der Meer *et al.* (1982) and de Lange *et al.* (1986). However, it is noteworthy that these studies only observed the time-evolution of the singlet character of the excited state $|\langle s|\psi(t)\rangle|^2$, and the dynamics in the triplet manifold $|\langle l|\psi(t)\rangle|^2$ remained to be examined.

Wang *et al.* (1999) revisited this classic problem by femtosecond time-resolved PEI to shed light on the dark triplet manifold. Photoelectron spectroscopy allows detection of both the singlet and the triplet states, thereby enabling direct observation of the intersystem crossing. Pyrazine in a molecular beam was excited to the S_1 0^0 level by a 324 nm femtosecond pump pulse and then subsequently ionized by a 197 nm femtosecond probe pulse. Ionization from the triplet state will produce low-energy electrons, since triplet levels isoenergetic with the initially photoexcited singlet 0^0 level have high vibrational energies (4055 cm^{-1} in the case of T_1). The Franck–Condon overlap therefore favours ionization to highly vibrationally excited states in the cation.

Figure 7 shows the photoelectron images observed at different pump–probe time delays. The cross-correlation between the pump and probe laser pulses is about 200 fs. The image observed at the shortest time delay consists of a number of sharp rings, however, this structure disappears with a lifetime of 110 ps. Correspondingly, a

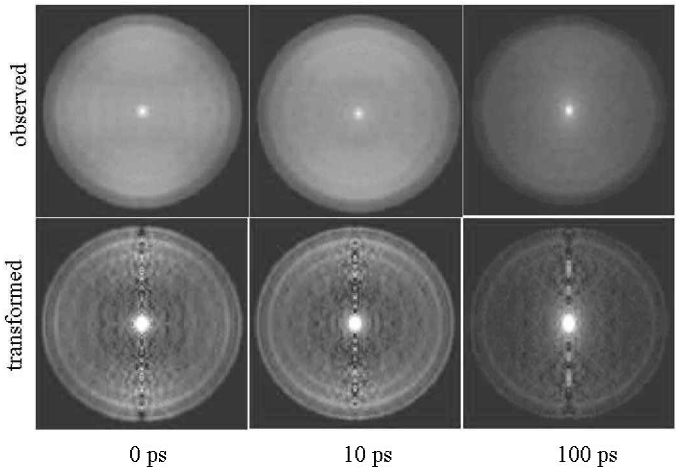

Figure 7. Photoelectron images observed at different pump–probe time delays for the $(1+1')$ photoionization of pyrazine via the $S_1\,0^0$ level. The upper images are the 'raw' images. The lower images are the corresponding Abel-transformed images.

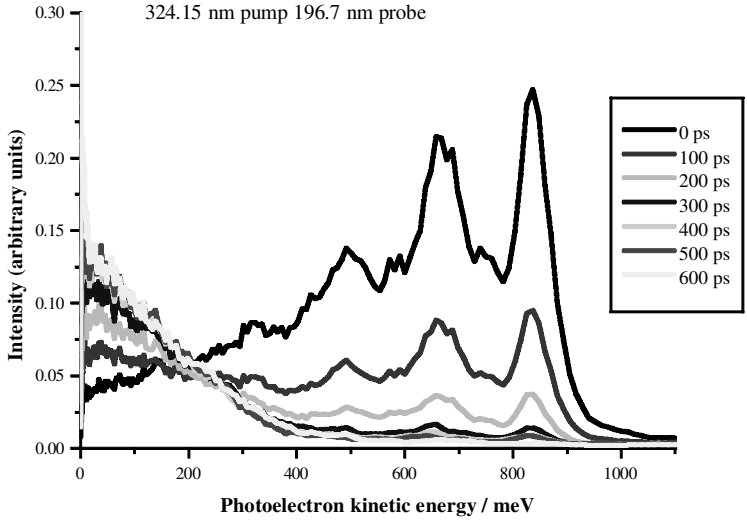

Figure 8. Photoelectron kinetic energy distributions deduced from images similar to those shown in figure 7.

low-energy electron signal grows in the inner part of the image. The sharp rings are transitions to vibrationally excited levels in the cation, and their intensity distribution follows the Franck–Condon overlap envelope between the $S_1\,0^0$ level and the cation. The observed lifetime, 110 ps, is in excellent agreement with the fluorescence decay lifetime of the fast component reported previously by McDonald *et al.* (1981), Yamazaki *et al.* (1983), Knee *et al.* (1985) and Lorincz *et al.* (1985). The pump and probe polarization directions are parallel, and in the vertical direction in the figure. The anisotropy of the PAD is observed to be rather small ($\beta \approx 0.3$).

The photoelectron kinetic energy distributions were determined from the images, as shown in figure 8. All the spectra cross at the same energy (isosbestic point),

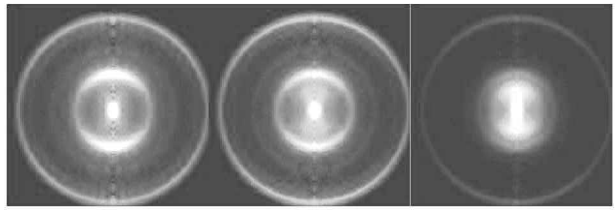

Figure 9. As the lower images in figure 7 but using a $(1+2')$ photoionization scheme via an intermediate Rydberg state.

indicating that the spectra consist of two components in dynamic equilibrium. The ionization from the triplet manifold peaks at zero kinetic energy indicating that 197 nm is not a sufficiently short wavelength to ionize the entire wave packet in the triplet manifold, making the sensitivity of the experiment to the triplet character relatively less than that for the singlet. We have excited pyrazine to various vibronic levels in S_1 ($E_{vib} < 2000\,cm^{-1}$) and observed the photoelectron images. In all cases, the singlet signal decayed without changing its structure, which means that IVR (or vibrational dephasing) in the S_1 manifold does not occur owing to the lack of sufficient vibrational state density. The same result has been obtained for deuterated pyrazine.

Pyrazine can also be ionized from S_1 by two-photon absorption of 401 nm light instead of one photon of 197 nm (Suzuki *et al.* 1999, Tsubouchi *et al.* 2001). Figure 9 shows the $(1+2')$ pump–probe photoelectron (Abel-inverted) images measured for pyrazine via the $S_1\,0^0$ level. The images are completely different from the $(1+1')$ case shown in figure 7. The observed images consist of three major rings with different radii corresponding to photoelectron kinetic energies of 40, 100 and 640 meV. The sharp ring structure indicates that all these ionization processes occur with the vibrational selection rule $\Delta v = 0$ via an intermediate Rydberg state at the energy of $\hbar(\omega_1+\omega_2)$. Strong anisotropy in the photoelectron image also points to atomic-like electron orbitals in the intermediate states. From comparison with the literature (see Innes *et al.* (1988) and references therein), the Rydberg states contributing to the two outer rings were assigned to the 3s (^1A_g) and 3p ($^1B_{3u}$ or $^1B_{2u}$) Rydberg states (figure 10). The intermediate state resonant in ionization of the triplet state has not been assigned yet.

The time dependence of the photoelectron intensity for the three rings (also shown in figure 11 (*a*)) are shown in figure 11 (*b*). The two outer distributions decay as a function of time ($\tau = 110$ ps) while the inner distribution grows with the same time constant, corresponding to the intersystem crossing from S_1 to the triplet manifold. More importantly, however, all these curves exhibit periodic revival structures. Note in particular that the structure appears in the photoelectron signal from the triplet manifold. These are assigned to periodic revival features of a rotational wave packet created by the coherent excitation of $\Delta J = 0, \pm 1$ ($\Delta K = 0$) transitions in the initial $S_1 \leftarrow S_0$ pump step.

We have analysed these features using the theory of RCS reported by Felker and Zewail (1987). For simplicity, we approximated the S_1 state of pyrazine as an oblate symmetric top; the A, B and C rotational constants are 6.1035, 6.0813 and 3.0477 GHz respectively (Innes *et al.* 1988). From other experiments we can fix the

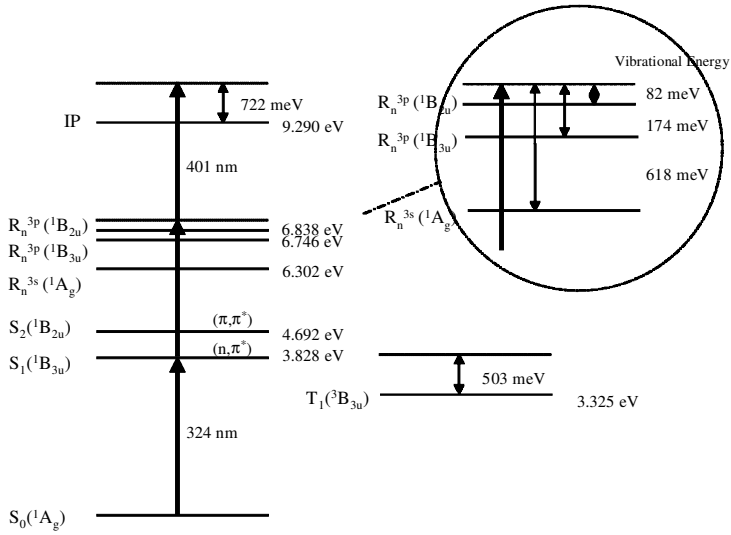

Figure 10. Energy level diagram illustrating the $(1+2')$ photoionization scheme for pyrazine and the vibrational energies expected on the basis of assignments by Innes *et al.* (1988). The inset shows an expanded view of the energy mismatch between the first photon and the origins of three intermediate Rydberg states.

rotational temperature, 20 K, of the sample and the intersystem crossing rate of S_1 to the triplet manifold, $9.1 \times 10^9\ s^{-1}$. By assuming the transitions from S_1 to R_n^{3s} and to R_n^{3p} to be parallel and perpendicular respectively, simulation of the RCS revivals agrees almost perfectly with observation, as shown in figure 11 (*b*). The transition from the S_1 ($^1B_{3u}$) to the 3p ($^1B_{3u}$ or $^1B_{2u}$) state is vibronically induced by excitation of the mode 11 (b_{3u}), making the transition to be a perpendicular type. The revivals in the triplet manifold were treated phenomenologically by assuming that the electronic dephasing occurs exponentially. The rotational constants known (Holtzclaw *et al.* 1989) for the $T_1\,0^0$ level were assumed for the triplet manifold. The revival peaks observed for the triplet state are, however, much weaker than simulation. Note that the number of triplet levels coupled to S_1 is estimated to be 20 states (Felker and Zewail 1986); so it is likely that slightly different rotational constants among these highly excited triplet vibronic levels cause the revival peaks to decrease.

As we have described already, the advantage of femtosecond pump–probe PEI is the capability to project the whole wave packet on to the cationic wavefunctions. However, the $(1+2')$ REMPI scheme no longer carries this feature, since Franck–Condon activity is reduced to a single peak by the resonance with the Rydberg states. What then is the advantage of $(1+2')$ photoelectron imaging? First of all, the lack of a Franck–Condon envelope avoids the overlap of photoelectron distributions from different electronic states, which otherwise makes it difficult to disentangle these components. Secondly, the angular anisotropy is quite high, and any variation in it can be more easily detected than for $(1+1')$ REMPI via a valence excited state.

Photoelectron images were recorded at pump–probe delay intervals of 500 fs around the positions of the half-revival at 41 ps and the first full revival of the rotational wave packet at 82 ps. At the full revival, the PAD exhibits a small enhancement in the direction of 90°. More quantitatively, the PAD measured at each time delay was fitted to the following form:

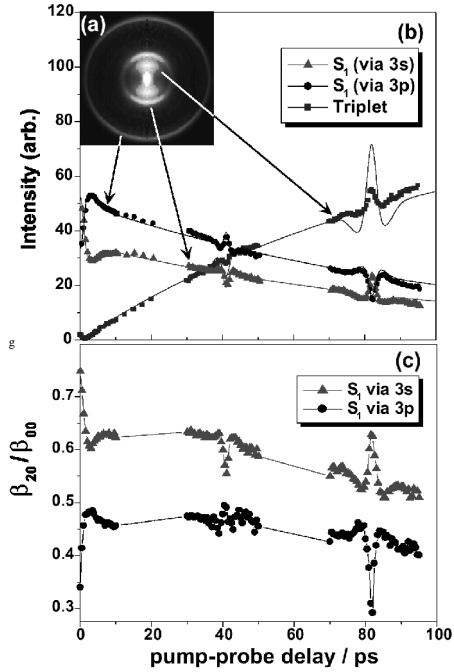

Figure 11. (*a*) Representative Abel-transformed photoelectron image obtained for the $(1+2')$ photoionization of pyrazine via the $S_1\ B_{3u}(n,\pi^*)\ 0^0$ level observed at a time delay of 30 ps. The original image was integrated for 80 000 laser shots. (*b*) Normalized time evolution of the ring structure shown in (*a*) recorded at 500 fs intervals for the angle-integrated intensities for the outer ring (kinetic energy, 643 meV) (●), middle ring (kinetic energy, 101 meV) (▲) and inner ring (kinetic energy, 37 meV) (■). The simulation taking into account the rotational coherence (——) is also shown. (*c*) The time evolution of the anisotropy for the two outer rings recorded for the $(1+2')$ PEI of pyrazine. The ratio β_{20}/β_{00} is related to the conventional anisotropy parameter β by $\beta_{20}/\beta_{00} = \beta/5^{1/2}$.

$$\frac{d\sigma}{d\Omega} = \beta_{00}\,Y_{00}(\theta,\phi) + \beta_{20}\,Y_{20}(\theta,\phi) + \beta_{40}\,Y_{40}(\theta,\phi) + \beta_{60}\,Y_{60}(\theta,\phi). \tag{14}$$

The ratio β_{20}/β_{00} thus obtained for ionization of S_1 via the 3s and 3p Rydberg states clearly shows the rotational revivals (figure 11 (*c*)).

In the $(1+2')$ case, the pump pulse creates a time dependent alignment $A_{20}(t)$ in the S_1 state, and the probe pulse transfers this alignment to rotational levels in the Rydberg states that ionizes instantaneously. Therefore, the PAD is ultimately modulated by the time dependence of $A_{20}(t)$ in the S_1 state.

The experimentally determined time-dependent PAD is also a means to access the PAD in the molecular frame. At time $t = 0$, the system maximally aligns the transition dipole moment to the pump laser polarization with a $\cos^2\theta$ distribution (one-photon absorption case). Specifically, the alignment is created by a parallel transition from S_0; so the principal axis of the molecule is aligned predominantly parallel to the pump laser polarization. Figure 12 (*a*) shows a polar plot of the PAD recorded by $(1+1')$ ionization measured with probe light at 201 nm aligned parallel to the pump laser polarization. The PAD at $t = 0$ shows a characteristic fourfold distribution that clearly indicates the photoelectrons are ejected not only along the

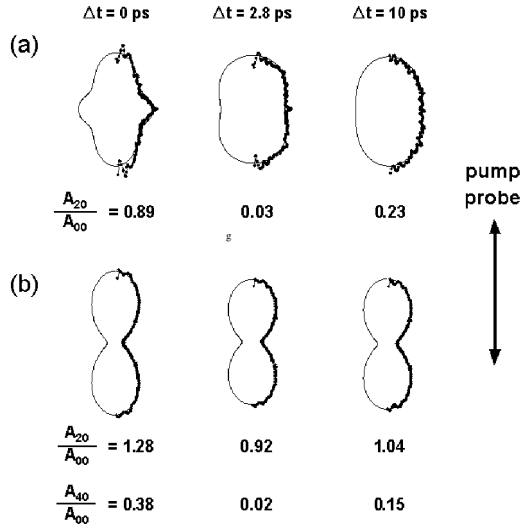

Figure 12. (*a*) Polar plot of the PAD observed for the $(1+1')$ photoionization of laser-aligned pyrazine via the $S_1\,0^0$ level. The probe light at about 200 nm is aligned parallel to the pump laser polarization. The pump–probe time delays and the alignment parameters are shown in the figure. Least-squares fits to the functional form given by equation (14) (——) are also shown. (*b*) as (*a*) but for the PAD recorded by $(1+2')$ ionization via the R^{3s} state measured with probe light at 401 nm aligned parallel to the pump laser polarization.

probe laser polarization (out of the molecular plane) but also perpendicular to it (in the plane). At 2.8 ps after the pump pulse the alignment parameter for pyrazine at the rotational temperature of 20 K almost vanishes, so the ensemble of molecules are randomly oriented in space. At this time, the characteristic fourfold feature also completely vanishes.

It is interesting to compare the PAD for ionization from different orbitals. The PAD observed by two-photon ionization of S_1 via 3s is interpreted as the PAD resulting from one-photon ionization of the 3s state aligned by $\omega_1+\omega_2$ two-step excitation from the S_0 state. The PAD measured for the 3s state shown in figure 12 (*b*) is dramatically different from that in figure 12 (*a*). At time delay $t=0$ between the pump ($S_1 \leftarrow S_0$) and probe laser pulses (ion $\leftarrow$ 3s $\leftarrow S_1$), the principal axis of pyrazine in the 3s state is maximally aligned with a $\cos^4\theta$ distribution with respect to the laser polarization. The corresponding PAD shows almost a $\cos^2\theta$ distribution, indicating that photoelectron ejection in the molecular plane of pyrazine is minimal. The time dependence of PAD is rather weak. This is because the probe laser pulse aligns and ionizes the 3s state within the pulse duration so that the alignment of the 3s Rydberg state of pyrazine is stronger than $\cos^2\theta$ at all times.

Both the S_1 and the 3s states have a hole in the n^+ (a_g) orbitals, and the outer electrons occupy $\pi^*(b_{3u})$ and 3s (a_g) orbitals, respectively. The difference between the PADs observed for the two cases can be ascribed to the different characters of the one-electron molecular orbitals (figure 13). The 3s orbital is atomic like and produces a predominant $p\pi$ outgoing wave in ionization, although the fact that β_{20}/β_{00} is smaller than its limiting value ($2/5^{1/2}$) indicates the deviation of the electron-core potential from centre symmetry. In contrast, the parallel transition of $\pi^*(b_{3u})$

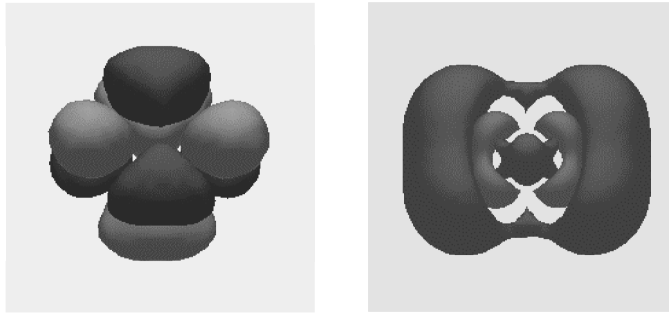

a b

Figure 13. Molecular orbitals calculated for the outer electron in (*a*) the S_1 state $\pi^*(b_{3u})$ and (*b*) the R^{3s} state $3s(a_g)$. The calculations were performed at the HF/6-311G(d, p) level of theory using the Gaussian98 package (Frisch *et al.* 1998).

requires outgoing partial waves of a_g symmetry. The result suggests that this a_g wave has some σ character along the z axis (through the N atoms).

4. Time-resolved photoion imaging

As we have seen in the previous section, photoelectron spectroscopy provides far richer information on the excited-state dynamics than mass spectrometry does. However, if the quantity of interest is the time-dependent population (concentration) of a particular chemical species, mass spectrometry is perfectly suited.

We consider here the unimolecular decay of a large molecule. The wave packet spreads over a large phase space volume, and the system tends to exhibit statistical behaviour. Experimental investigations of these sorts of reactions are mainly based on the measurements of reaction rates and comparison with statistical theories such as Rice–Ramsperger–Kassel–Marcus (RRKM) theory (Baer and Hase 1996, Holbrook *et al.* 1996). Experimentally, unimolecular reactions can be initiated by various energization methods, such as shock tubes, infrared multiphoton excitation, overtone excitation, electronic excitation followed by internal conversion and, more recently, stimulated emission pumping. However, the method has been rarely applied to free radical species because of the experimental difficulty, even though radicals may exhibit interesting non-RRKM behaviour as a result of their low reaction energy barrier.

Ideally, we need an experimental method that allows efficient formation of radicals in a range of highly excited states and measures the subsequent decay for each internal energy. A novel experimental method that includes these two features is time-resolved photoion imaging (Shibata and Suzuki 1996). The principle is explained in figure 14. The radicals *R* are produced by photodissociation of molecules R–X in a molecular beam. Following irradiation by the pump laser pulse, radicals are ejected from the molecular beam with various internal energies. With a certain pump–probe delay, these radicals are interrogated by multiphoton ionization using a probe laser pulse. When the atom X is created in a single quantum state, the translational energy of the radical R is related to the internal energy of R through the energy and momentum conservation laws. Then, radicals with low internal energies have a high translational energy and are deflected far from the molecular beam, while radicals with a high internal energy have a lower

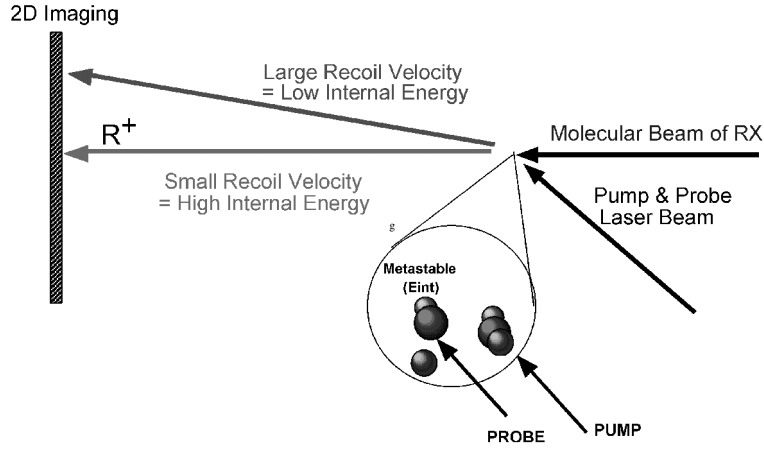

Figure 14. Illustration of the principle behind imaging the unimolecular decay of metastable radicals. The radicals R are produced by photodissociation of molecules R–X in a molecular beam. By irradiation of the pump laser pulse, radicals are ejected into space with various internal energies. With a certain pump–probe delay time, the radicals are interrogated by multiphoton ionization by a probe laser pulse.

translational energy and remain close to the molecular beam. In this way, radicals with different internal energies are dispersed in space and can be detected by a 2D position-sensitive detector. If the radical has sufficient internal energy to surmount the barrier for secondary dissociation, $R \rightarrow A + B$, it will decompose before being ionized by the probe laser pulse. Disappearance of radicals with a certain translational energy can therefore be visualized by 2D ion imaging, so that a series of ion images taken by varying the pump–probe delay allows observation of the unimolecular decay of energy-dispersed radicals. Time-resolved observation of metastable radicals produced by photodissociation has been reported before by Kim *et al.* (1995, 1996), Kim and Zewail (1996) and Owrutsky and Baronavski (1999). The novel feature of the technique based on ion imaging, however, is the dispersion of the radical R with different internal energies, which is the key with which to unlock the connection between the decay rate and the internal energy E.

The 2D image of CH_3CO produced by 255 nm photodissociation of CH_3COCl is shown in figure 15 (*a*). The pump–probe time delay is 10 ps. It is clear that the CH_3CO radicals are ejected primarily parallel to the pump laser polarization. The angular distribution (figure 15 (*b*)) was fitted to the standard formula (equation (1)), which yielded an anisotropy parameter $\beta = 0.9 \pm 0.1$ in agreement with previous studies (Person *et al.* 1992). The centre-of-mass translational energy release $P(E_T)$ resulting from the C–Cl bond rupture is shown in figure 15 (*c*). It was found to accord with the literature value (North *et al.* 1994).

Ion images of CH_3CO as a function of pump–probe time delay were measured. From these the translational energy distribution of acetyl radicals was obtained, that is the internal energy distribution of 'surviving' acetyl radicals. Figure 16 shows the decay of acetyl radicals with particular translational energies. Because of the fine-structure branching of Cl into $^2P_{1/2}$ and $^2P_{3/2}$ states (separated by 10.26 kJ mol^{-1}), each translational energy corresponds to two different internal energies of the acetyl radical, as indicated in the figure. According to Deshmukh and Hess (1994), the fine-

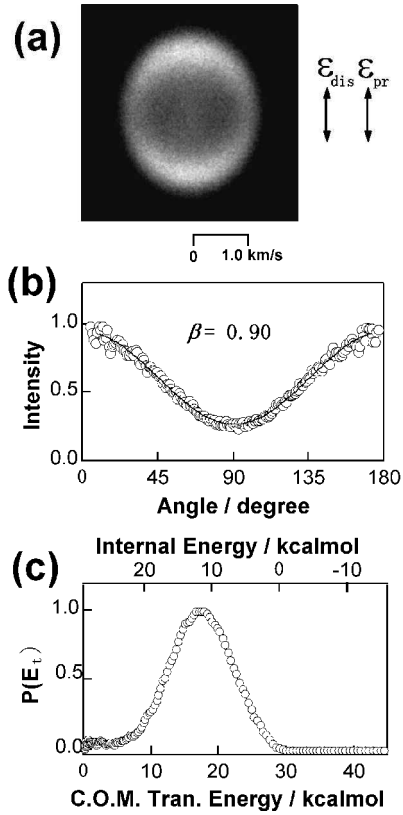

Figure 15. (*a*) The 2D image of CH_3CO produced by 255 nm photodissociation of CH_3COCl recorded at a time delay between the pump and probe lasers of 10 ps. The relative orientations of the laser polarizations are both aligned vertically in the figure. The image was accumulated for 140 000 shots. (*b*) PAD of the CH_3CO radical deduced from (*a*) at the centre-of-mass translational energy release of 14.6–20.2 kcal mol^{-1}: (——), least squares fit to equation (1). (*c*) Centre-of-mass (C.O.M.) translational (Tran.) energy release in 255 nm photodissociation of CH_3COCl. The internal energy distribution of the CH_3CO radical, when it is produced with $Cl(^2P_{3/2})$ channel, is also indicated in the figure.

structure branching [Cl*]/([Cl*]+[Cl]) is 0.4 at 236 nm. Even with this slight complication, figure 16 clearly shows that the radicals with higher internal energies decay faster. More quantitatively, the decay rates at each internal energy have been estimated by least-squares fitting of single- or double-exponential decays to each plot. The observed rate was nearly one order of magnitude smaller than the RRKM calculations (figure 17).

The discrepancy is thought to be due to restricted IVR and rotational metastability. If the initial internal energy is partitioned into vibrational modes that are poorly coupled to the C–C stretching modes, IVR becomes incomplete, leading to a smaller reaction rate than predicted by RRKM theory. As for the latter possibility, since acetyl chloride becomes pyramidal in the $^1(n, \pi^*)$ state, C–Cl repulsion is expected to excite molecular rotation of CH_3CO around the *a* axis. The *a*-axis

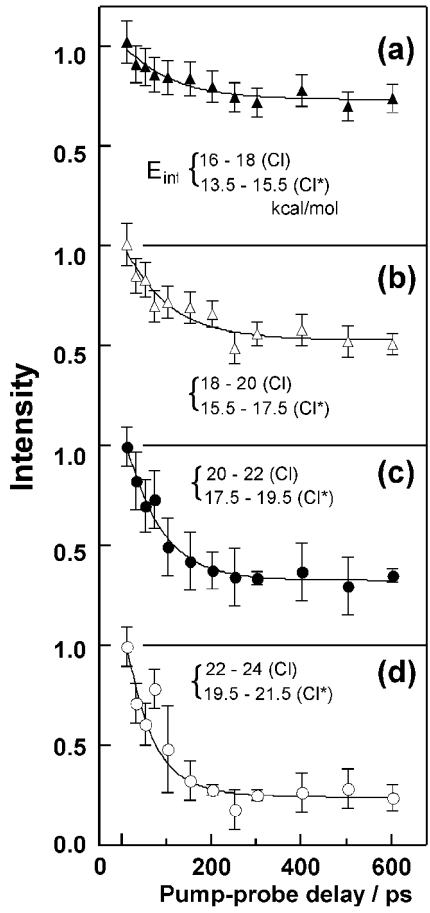

Figure 16. CH_3CO radicals with different internal energies observed by varying the pump–probe time delay. Note that each translational energy corresponds to two internal energies of the acetyl radical due to the two possible spin–orbit states of Cl atoms: (a) 17 ± 1 and 14.5 ± 1 kcal mol^{-1}; (b) 19 ± 1 and 16.5 ± 1 kcal mol^{-1}; (c) 21 ± 1 and 18.5 ± 1 kcal mol^{-1}; and (d) 23 ± 1 and 20.5 ± 1 kcal mol^{-1}. (For comparison with the energies in the text, 1 kcal mol$^{-1} \equiv 4.18$ kJ mol^{-1}.)

rotation is poorly coupled with the reaction coordinate and, if K scrambling is restricted, it will make CH_3CO rotationally metastable.

Recently, Martinez-Nunez and Vazquez (2000) have investigated this process for the same energy range by classical trajectory calculations. They found intrinsic RRKM behaviour for the dissociation with zero total angular momentum. However, when molecular rotation is excited around any of the three principal axes the dissociation rate decreased irrespective of the direction of rotational axis. In addition, torsional excitation of methyl group diminished the dissociation rate significantly. At 96 kJ mol^{-1} and for 6.7 ps, which is the average lifetime at this energy, K scrambling was found to be 15–40%, suggesting that the rotation–vibration coupling is fairly weak. Thus, they concluded that torsional excitation of CH_3 and a-axis rotation are the cause of the observed non-RRKM behaviour, in accord with the earlier speculation.

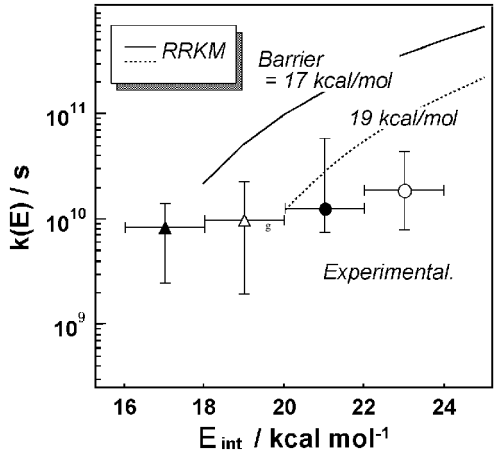

Figure 17. Comparison of two model RRKM calculations assuming different barrier heights with the experimentally determined microcanonical unimolecular rate constants for acetyl radicals.

5. Coulomb explosion imaging

Originally, CEI was used to refer to experiments in which a fast ion beam (about 10 MeV) collided with a thin (approximately 100 Å) foil target (see Vager *et al.* (1989) for a review and Levin *et al.* (2000) for details of target materials). In a later refinement, accelerated anions are first neutralized by electron photodetachment (Kella *et al.* 1993). In either case, the rapid transit (about 0.1–1 fs) of the ion or neutral through the target induces nearly instantaneous stripping of the binding electrons. The resulting fragments are generally multiply charged ions. They are created at distances where, now in the absence of the shielding effects of the binding electrons, they experience a strong mutual Coulomb repulsion and hence repel each other. This process is known as a Coulomb explosion.

By measuring the arrival time and position of each ion fragment from a series of molecules hitting the foil target one is able to build up a picture which maps (by means of a so-called Bayesian deconvolution) on to the distribution of nuclear configurations in the measured molecular ensemble (Zajfman *et al.* 1992, Levin *et al.* 1996). In this way, one is able to deduce the average molecular structure and the nature of excursions from the equilibrium geometry. Such studies have provided important structural information about 'floppy' molecules and ions, which are difficult to characterize by conventional spectroscopic methods (Zajfman *et al.* 1992), and can even be used to study reaction intermediates (Levin *et al.* 1998).

Note that, in this type of experiment, one has to record simultaneously the arrival times *and* positions of the fragment ions arising from the Coulomb explosion in order to recover the molecular geometry. For this reason, it is not possible to use MCP or phosphor-type detectors on their own as these give only good position information. The most common type of detectors for CEI are wedge-and-strip anode, resistive anode or delay lines as in ion–photoelectron coincidence experiments. There is currently considerable research effort under way to improve the response time of these detectors and hence the number of particles whose velocities can be correlated in a single shot. One way this can be done is to record simultaneously the arrival time of each fragment with a photomultiplier tube and

the spatial image recorded with an MCP or phosphor (Amitay and Zajfman 1997). Another is to employ a MCP or CCD camera particle detector that utilizes Au strips deposited upon the surface of a MCP to provide particle arrival time information (Rosen *et al.* 1998).

As a result of the development of Kerr-effect self-mode-locked Ti:sapphire lasers and chirped pulse amplification there is, however, another way to induce a Coulomb explosion. It has recently become possible to generate laser pulses with terawatt peak powers on a laboratory table-top (see Backus *et al.* (1998) or Reid and Wynne (2000) for recent review articles). The development of these lasers provides pulses in which the peak electric field is of comparable magnitude with the internal fields which bind electrons to atomic nuclei. For example, a 30 mJ pulse in 30 fs attains a peak power of 1 TW. The diffraction-limited beam waist is likely to be of the order of 10 μm; so the effects that we are about to describe can be achieved with more modest lasers. However, by focusing to a waist of about 100 μm the laser field can be more easily matched to the typical dimensions of a molecular beam. For a beam waist of 100 μm, then, the intensity peaks at about $3 \times 10^{19}\,\mathrm{W\,m^{-2}}$. In SI units the intensity I is related to the electric field strength E (assuming linearly polarized light) by

$$I = c\varepsilon_0 E^2; \tag{15}$$

so the electric field at the focus is of the order of $10^{11}\,\mathrm{V\,m^{-1}}$ or $10\,\mathrm{V\,Å^{-1}}$. This is comparable with the field F_a binding the electron to the nucleus and means that it is possible to perform the CEI experiment using light rather than a metal foil to induce the Coulomb explosion. To distinguish the latter from the former we shall refer to laser-induced Coulomb explosion (LICE).

There is no unique definition of the atomic field (Delone and Krainov 1994). One is to consider the Coulomb field experienced by a H 1s electron at a distance a_0 from the nucleus

$$F_a = \frac{1}{(4\pi\varepsilon_0)^3}\frac{m_e^2 e^5}{\hbar^4} \approx 5 \times 10^{11}\,\mathrm{V\,m^{-1}}, \tag{16}$$

but a more useful definition is to take F_a as the maximum of the effective potential barrier equal to the ionization potential E_i. For hydrogenic atoms then

$$F_a = \frac{1}{(4\pi\varepsilon_0)^3}\frac{Z^3}{16n^4}\frac{m_e^2 e^5}{\hbar^4}, \tag{17}$$

which for hydrogen is one sixteenth of that given by equation (16).

The ionization process is clearly nonlinear since the photon energy is much less than the ionization energy of the molecule. For lower intensity fields, achievable say with Q-switched or actively mode-locked laser systems, the ionization process can be viewed as a multiphoton transition via a series of 'virtual' states to the continuum. However, as the laser intensity increases, direct tunnelling ionization becomes possible as the electric field strength of the light becomes comparable with the atomic or molecular field. The process is complex and no analytical solution exists to describe the quantum mechanics fully. The interaction physics in simple atoms can be solved numerically but more insight is gained from an approximate approach first introduced by Keldysh (1964) and later extended by Reiss (1980) and others (see for example Delone and Krainov (1994)). A crucial parameter in these models is the ratio of the ionization to ponderomotive potential. The latter is essentially the ac

Stark shift (Dietrich *et al.* 1993). This parameter is known as the adiabaticity or, more commonly, the Keldysh parameter

$$\gamma = \frac{\omega}{eE_0}(2mE_{\mathrm{IP}})^{1/2}, \tag{18}$$

where E_0 is the peak field of the light at angular frequency ω, e and m are the electron charge and mass respectively, and E_{IP} is the ionization potential. If $\gamma^2 \gg 1$, the rate w of nonlinear ionization depends on E_0 to some power, which can be interpreted as the number of photons involved in the transition, while, if $\gamma^2 \ll 1$, tunnelling dominates and the rate of nonlinear ionization depends exponentially on the field strength:

$$w \propto \exp\left(-\frac{2(2E_{\mathrm{IP}})^{3/2}}{3E_0}\right). \tag{19}$$

The intermediate range of $\gamma^2 \approx 1$ is a narrow region as a function of ω or E_0 and is generally not considered.

The underlying assumption behind the Keldysh approach is that the transit time of the electron across the atom as it responds to the applied field of the laser is fast with respect to the pulse duration. This is the adiabatic approximation again. As we shall see in molecular systems, in which the electron is effectively delocalized over the entire molecule, this approximation is likely to break down. Stolow (1999) has considered this point in more detail.

From the early 1990s the LICE of diatomic molecules, such as N_2, CO and I_2 (Posthumus *et al.* 1996), triatomic species including CO_2 (Cornaggia *et al.* 1994), SO_2 and NO_2 (Hishikawa *et al.* 1998b), and even some polyatomic species, $C_3H_4^+$ (Cornaggia 1995), began to be studied. It was soon apparent that the interpretation of the results of these experiments were not as straightforward as the experiments with thin foils (Codling and Frasinski 1994).

The additional nuclear degrees of freedom in molecules, compared with atoms, lead to a number of interesting phenomena, such as above-threshold dissociation, laser-induced avoided crossing and charge-resonance spectra, analogous to plasmon effects in macroscopic systems (Bandrauk *et al.* 1993). However, the simplest description of the intense field ionization occurring in a LICE is very similar to that in atoms with the slight complication that the ionization potential barrier depends on the relative orientation of the nuclear framework with respect to the light field. Thus one expects to see polarization effects. This model is partially successful in explaining the ionization and subsequent fragmentation of heavy molecules, such as I_2, but the details do not fit exactly. The fragmentation dynamics of the lighter molecules such as N_2 and CO do not fit the model at all. It is found that the translational energies of the fragments are systematically lower than would be predicted by the model if it is assumed that the molecule is ionized from its (generally known) equilibrium geometry. This appears to be true for all the observed fragmentation channels, as deduced from covariance mapping (Frasinski *et al.* 1991, 1992), or other techniques (Hishikawa *et al.* 1998a). Furthermore, the kinetic energy release is relatively insensitive to other experimental parameters such as laser wavelength or pulse duration. The fragment energies are consistent with a field ionization model but at internuclear distances greater by 20–50% than the equilibrium values.

There are several explanations for this effect. Bandrauk *et al.* (1999) proposed that at critical bond lengths and angles the ionization rate is enhanced above that expected from the field ionization model due to large Stark shifts of the lowest unoccupied molecular orbitals. In other versions of events the molecules experience enhanced ionization rates when they are aligned with respect to the laser applied field, evidence for which comes from the laser polarization dependence of the kinetic energy release (Hering and Cornaggia 1999). Yet others (Brewczyk and Rzazewski 1999) argued that the kinetic energy defect is due to the screening effect of the departing electrons. The approach of Brewczyk and Rzazewski (1999) which is based on a Thomas–Fermi electron gas model has appeal for chemists because of its links to density functional theory, however, the predictions of the ionization rate have so far only been made for linearly polarized light (for which the agreement with experiment is very good) and will need to be checked against the experimental results for circular polarization.

Given this uncertainty in the interpretation it is perhaps surprising that the technique is being increasingly applied to the study of molecular dynamics. What then is the advantage of LICE for molecular dynamics studies? As described in the introduction, molecular dynamics is concerned with trying to understand the changes occurring to the molecular structure during the course of a chemical reaction. The most powerful techniques, to date, for determining molecular structure are spectroscopic. High-resolution laser spectroscopy, in particular, has been extremely successfully applied to determine, with high precision, the near-equilibrium geometries of the low-lying electronic states of even quite complicated small molecules (Pratt 1998). Spectroscopic methods can also be used to probe molecules away from their equilibrium geometry, as we have seen in the case of photofragment spectroscopy, by exciting molecules to non-stationary states. More recently, as we have also seen, femtosecond pump–probe techniques allow us to probe the time evolution of a molecular wave packet.

However, the interpretation of these experiments is limited by the necessity to know something about the topography of the PESs involved. Recall that in these experiments, such as the prototypical experiment on NaI by Rosker *et al.* (1988), the time evolution of the (nuclear) wave packet on the excited-state surface is probed by using a second time-delayed femtosecond pulse to project this wave packet on to a third state. In the NaI experiment the final state is Na(^{2}P) from which fluorescence can be observed. The experiment works because the Franck–Condon overlap between quantum states on the final surface and the moving wave packet on the intermediate surface evolves with time. This, however, means that, in general, one needs to know the shape (curvature) of the PES of the final state involved *a priori* to invert the data and to obtain an understanding of the *geometry* changes that the nuclear framework in the intermediate state is undergoing.

We are seeking a method capable of resolving the motion of the nuclear framework through the transition state region of a chemical reaction. That is, a technique capable providing time-resolved structural information on a femtosecond time scale. Technology is just becoming available which allows us to observe the nuclear motion directly. For example, ultrafast lasers are capable of generating pulsed electron beams and X-rays that can be used in time-resolved electron or X-ray scattering experiments on the vibrational time scale (Barty *et al.* 1996). One such example is the observation of the time evolution of the X-ray absorption spectrum near the K edge of S atoms around 2.48 keV following the photodissociation of

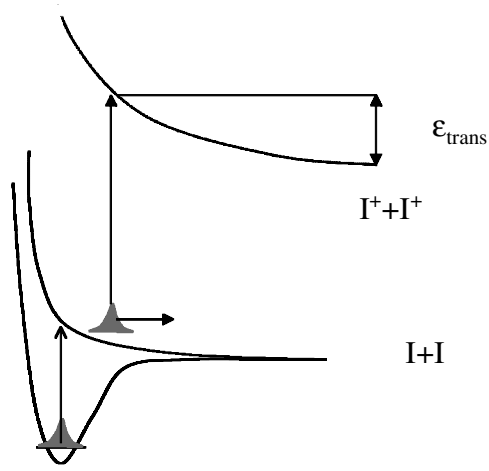

Figure 18. Illustration of the principle behind the experiment described by Larsen *et al.* (1998). A femtosecond pump pulse creates a vibrational wave packet on the $A\,^3\Pi_{1u}$ state of I_2. The subsequent time evolution is probed by a delayed intense probe pulse, which excites the wave packet to the $I^+ + I^+$ Coulomb potential. The kinetic energy release in the I^+ fragments is measured by CPI.

gaseous SF_6 (Raksi *et al.* 1996). Cao *et al.* (1999) and Williamson *et al.* (1997) have investigated the use of ultrafast electron diffraction and have been able to observe the transient intermediate in the elimination reaction of 1,2-diiodotetrafluoroethane to tetrafluoroethylene. In the same vein, Stapelfeldt *et al.* (1995) and Ellert *et al.* (1998) have suggested the possibility of using LICE in a pump–probe mode to image an evolving nuclear wavefunction, and it is this we concentrate on here.

There have been several experiments which have demonstrated the application of LICE to nuclear wave-packet imaging. Stapelfeldt *et al.* combined LICE and CPI to record Coulomb explosion snapshots of a wave packet propagating on the $A\,^3\Pi_{1u}$ surface of molecular I_2 (Larsen *et al.* 1998). A schematic diagram of their experiment is shown in figure 18. The wave packet is prepared by a weak femtosecond pump which excites I_2 molecules from the ground $X\,^1\Sigma_g^+$ state to the A state. The pump laser at about 670 nm has a peak intensity of about 4×10^{12} W cm^{-2} and a duration (cross-correlation with the 800 nm main beam) of 100 fs. The A state of I_2 is dissociative and so the wave packet initially created evolves outwards to larger internuclear separation. At controlled time delays the wave packet is probed by LICE using the remaining approximately 800 nm output of the amplified Ti:sapphire laser. The probe beam in these experiments is about ten times more intense than the pump beam.

The ions produced by the probe beam are extracted by an electrostatic lens using the velocity mapping configuration (Eppink and Parker 1997) and projected on to a MSP backed by a phosphor screen at the end of a drift tube. Ion images, mass gated on the I^+ fragments, were recorded as a function of the pump–probe delay. The images clearly show the evolution of the internuclear separation of the dissociating I_2 molecule; at relatively short pump–probe delays a large-diameter ring is observed; the diameter of this ring decreases with increasing pump–probe delay because at larger internuclear separations the Coulomb repulsion energy between the two I^+ fragments is reduced (see below). At the centre of the images a small-diameter ring is

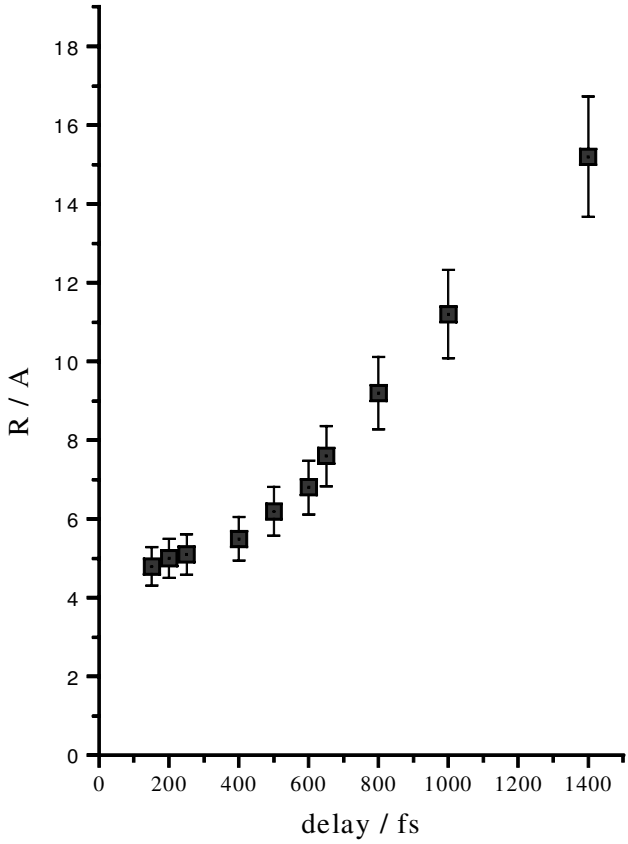

Figure 19. The I...I internuclear distance as a function of time measured by pump–probe LICE for a dissociating nuclear wavefunction propagating on the $A\,^3\Pi_{1u}$ state of I_2. The data are redrawn from the results of Larsen *et al.* (1998).

also always observed. Its diameter does not change with the pump–probe delay time and it is identified with ionization of I_2 to $I...I^+$. The velocity of the I^+ in this channel only depends on the recoil energy, that is on the energy difference between the photon and the dissociation asymptote. For the $I_2 \rightarrow I^+ - I^+$ ionization channel the kinetic energy of each of the I^+ ions is given by the sum of the recoil energy E_d and half the Coulomb energy; so, from the measured velocity v_r of the I^+ fragments one can deduce the bond length at the moment of ionization:

$$R(t) = e^2 \Big/ 8\pi\varepsilon_0 \left(\frac{m v_{I^+}^2}{2} - E_d \right). \tag{20}$$

The time dependence of the internuclear separation so measured is reproduced in figure 19. Since the shape of the $A\,^3\Pi_{1u}$ surface is well known from previous high-resolution spectroscopy work (see for example Tellinghuisen (1973)) it is possible to solve the time-dependent Schrödinger equation for this system and so to compare the experimental and 'true' wave-packet dynamics.

In general the experimental results are in good agreement with the quantum-mechanical wave-packet simulations. For example, the experimentally determined

asymptotic internuclear velocity is 9.3 Å ps^{-1} in comparison with a calculated value of 9.7 Å ps^{-1}. On the other hand, there are some important differences between the calculated and experimentally observed wave packets. For example, the experimental wave packet is twice to four times wider than the calculated value. Two factors were thought to be responsible for this: the finite duration of the probe pulse and the velocity spread in the initial molecular beam. With a faster laser and by imaging on the axis of the molecular beam it should be possible to minimize these effects and perhaps to reach an internuclear resolution of the order of one tenth of an ångstrom or less. This would be sufficient to enable precision measurements of the detailed structure of wave packets to be made.

The conversion of the observed velocity distribution into a radial distribution requires that the ionic surface excited by the probe pulse is truly Coulombic. We anticipate that for pump–probe LICE experiments at early times, when the internuclear distance is small, this condition is likely to break down. For internuclear separations less than about 4.5 Å in I_2 the I_2^{2+} curve deviates from $1/R$ behaviour because of the effects of covalent bonding (Constant *et al.* 1996, Corkum *et al.* 1997). At these short distances, LICE cannot faithfully map (image) the nuclear wavefunction because it is not valid to assume a simple Coulombic potential for inverting the kinetic energy distribution in order to recover the nuclear wavefunction.

Chelkowski *et al.* (1999) have discussed the limitations of LICE imaging of vibrational wavefunctions (in the sense of measuring the square of the probability density function). They show that there is, in general, no simple means of recovering the vibrational wavefunction $\Psi_{\mathrm{LICE}}(R)$ from the kinetic energy spectrum $S(E)$ of the fragments. However, in the limit of a truly Coulombic final state and zero initial kinetic energy the Jacobian $|\mathrm{d}E/\mathrm{d}R|$ is obviously q^2/R^2 (q is the ionic charge and the equation is in atomic units) so that

$$|\Psi_{\mathrm{LICE}}(R)|^2 = |S(E)|\frac{q^2}{R^2}. \tag{21}$$

From exact non-Born–Oppenheimer simulations of the dissociative ionization of H_2^+ in an intense laser field they compared the 'real' vibrational wavefunction with that recovered from the modelled Coulomb explosion.

In model calculations with a Coulomb field of 4×10^{19} W m^{-2} the agreement between the input and recovered wavefunction is good but not perfect. However, by considering He_2^{3+} imaged on to the $He^{2+}\ldots He^{2+}$ Coulomb surface Chelkowski *et al.* (1999) showed that most of the distortion arises from the neglect of the momentum associated with the input wavefunction $\Psi_{\mathrm{in}}(R)$ in the reconstruction process. Chelkowski *et al.* (1999) concluded that the vibrational wavefunctions of larger mass molecules than H_2^+ with Coulomb-like dissociative states, for example Na_2^{2+} and Ca_2^{4+}, should be amenable to LICE imaging. For non-closed shell ions, the effects of electron correlation cannot be neglected and the vibrational wavefunction is not directly recoverable using a classical Coulomb explosion theory. However, this might be a way of investigating the configuration interaction directly since for many first- and second-row diatomic molecules we already have detailed information about the PESs from conventional spectroscopy. Therefore, by comparing the Coulomb explosion images with the known vibrational wavefunctions we might hope to gain information on the electron correlation effects. In the light of the recent impact of density functional theory on quantum chemistry and the theoretical

work of Brewczyk and Rzazewski (1999) this might be a fruitful line of future research.

In a somewhat different vein, Folmer *et al.* (1998, 1999) have recently investigated proton transfer in the 7-azaindole dimer by pump–probe Coulomb explosion, although the interpretation of their results has been disputed (Catalan *et al.* 2000, Folmer *et al.* 2000). Proton transfer in the 7-azaindole dimer has for some years been considered a model system for the proton-transfer-induced tautomerization of deoxyribonucleic acid base pairs and hence mutagenesis (Taylor *et al.* 1969). The question is: does the double proton transfer in these model base pairs proceed in a stepwise or concerted fashion? Douhal *et al.* (1995), using two-colour pump–probe femtosecond spectroscopy, observed biexponential temporal transients in the TOF mass spectrometer, which suggested a sequential mechanism. Folmer *et al.* (1998) attempted to verify these results by direct observation of the transient intermediate species by pump–probe LICE. A weak-intensity pump laser at about 312 nm initiates the proton transfer reaction in a molecular beam containing 7-azaindole dimers. The transient intermediate is probed by a 2 mJ, 120 fs pulse at about 624 nm, which induces a Coulomb explosion in the intermediate. If only one proton has transferred, one expects to see ion fragments of 119 and 117 amu whereas, before initiation and after both protons have transferred, the dimer is expected to fragment into two moieties each of mass 118 amu. Folmer *et al.* (1998) did indeed observe a transient in the 119/118 mass-ratioed TOF mass spectrometer signals with a rise time and a decay time that were broadly in agreement with the transients observed by Douhal *et al.* (1995). However, the expected 117 amu mass is absent (it is suggested that this explodes into much smaller fragment ions, although why this should occur for one moiety and not the other is unclear). Supporting evidence for the claim that LICE is observed in the experiment comes from the fact that the TOF spectrum of the 119 and 118 amu mass fragments of the exploded dimer are broader than the TOF mass peaks at 119 and 118 amu recorded at lower backing pressures and therefore in the absence of dimers in the beam. The broad peaks are indicative of kinetic energy release and hence support the Coulomb explosion interpretation of the data. Although it is also possible that the broadening might be due to space-charge effects and further experiments are undoubtedly required.

6. Future directions and conclusions

If the electronic motion and the nuclear motion are decoupled, as is considered to be the case in the Born–Oppenheimer approximation, chemical dynamics can be described in terms of the motion of a particle (wave packet) over a single PES. After nearly 50 years of experimental and theoretical work, such *adiabatic* dynamics are now well understood. Major effort should now be directed towards the elucidation of 'realistic' chemical dynamics without such an oversimplification. Indeed, non-adiabatic (or non-Born–Oppenheimer) dynamic effects are not an exception but are rather a common feature in the dynamics of large polyatomic molecules and in the condensed phases, because of the existence of a number of electronic states that are nearly energetically degenerate.

Femtosecond pump–probe spectroscopy combined with CPI offers great insight into the non-adiabatic dynamics of chemical reactions. At least, two types of experiment are now possible: time-resolved PEI and (pump–probe) LICE.

Pump-probe photoelectron spectroscopy is able to follow both the electron and the nuclear dynamics throughout the course of a chemical reaction by projecting the wave packet on to cationic PESs. By using several cationic electronic states as templates for the electronic configuration, as originally proposed by Seel and Domcke (1991), we have seen how it is possible to unravel the rapid change in the electron configuration around a crossing region of coupled PESs. In this vein, coincidence detection of photoelectrons and ions using dissociative ionization as a probing step provides further detailed information, such as the PAD in the molecular frame. However, it has to be kept in mind that this approach is only applicable to small molecules that dissociate almost instantaneously upon ionization and will not work with complicated molecules and clusters. Non-coincidence PAD measurements on aligned molecules, as we have demonstrated for pyrazine, will be a more general approach to this problem.

The LICE experiment is not sensitive to the electron dynamics but, on the other hand, it is capable of determining the nuclear geometry, and hence the nuclear wavefunction, without any *a priori* knowledge of the PESs. This is a major advantage but only true if the molecule explodes with pure Coulombic repulsion between the atomic ions. Such a simple picture is unlikely to be realized at short bond distances, because of the exchange interaction between the atomic ions. Nevertheless, the technique should be applicable to the investigation of nuclear wave-packet bifurcation in the exit channel, for example in methyliodide.

Current ultrafast lasers work most stably and efficiently at about 1 kHz repetition rate. This means that the read-out frequency of an ordinary video rate camera (25 or 30 Hz) is too low to perform centroiding and thresholding calculations on a shot-to-shot basis. CMOS detector technology appears to be one of the solutions for obtaining faster read-out times. Electronic position-sensitive detectors are also capable of detecting charged particles at high count rates, and they are still very useful. However, the inherent multiplex capability of camera-based imaging detectors is advantageous in the case where a relatively large number (more than four or five) of charged particles arrive at the detector almost simultaneously. In laser experiments this is often the case, since even with a 1 kHz laser the duty cycle is still low and much of the experimental acquisition time consists of the 'dead time' waiting for the next laser pulse and all the signal must be concentrated into a time window of less than a few tens of nanoseconds.

The recovery algorithms needed to obtain a cylindrical symmetric 3D distribution from its 2D projection are now well established. It is a quite natural step, however, to develop direct 3D measurements based on the simultaneous measurement of the arrival position and time of the charged particles. Such an advance would obviate the tedious numerical inversion procedure and, more importantly, would provide far more flexibility in the experimental arrangement. If the directions of the pump–probe laser polarization and image projection were not constrained by the necessity of obtaining an Abel-invertible image it would be experimentally easier to probe vector properties, such as **v**–**J** correlations, in the reaction products. Electronic detectors capable of doing this have already been built but are in their infancy. An interesting recent development involves the use of a mask to cover alternate rows of a CCD chip. By rapidly dragging the charge from the exposed region of the CCD chip into the masked region, two very rapid exposures can be made and thus the charge cloud can be imaged at two different times as it passes through the detector plane. From such measurements, it would be possible to build

up a picture of the 3D velocity distribution directly. This would be advantageous, since there is virtually no limitation in the number of particles that can be detected in each exposure, unlike the electronic detectors.

We have described two general experiments with which to examine the details of the molecular wavefunction in regions close to surface crossings. To examine the wavefunction even more closely it would be nice if we could lock the molecule's frame of reference to our laboratory frame. How about tweezers? Control of the alignment of molecules with a permanent dipole moment by strong static electric fields has been practised for sometime (Loesch 1995). More recently the anisotropic interaction of an intense non-resonant laser field with the induced dipole moment in a molecule has been used to align the molecule with respect to the polarization vector of the light (Kim and Felker 1996, Sakai *et al.* 1999) (see also Corkum *et al.* (1999) for a overview of the potential of strong laser fields to control molecular orientation and other parameters, such as velocity, of interest in molecular reaction dynamics and stereochemistry). When the pulsed strong laser field creates a rotational wave packet from a number of J levels, the rotational revival by constructive interference after the laser pulse results in an sharply peaked alignment distribution. This ensemble of molecules will be an ideal target from which to obtain molecule-fixed PADs. Seideman (1999) has performed model calculations in which NO molecule is aligned by an intense femtosecond pump pulse and the PAD is interrogated by a subsequent femtosecond probe pulse. Vrakking (2001) has demonstrated non-resonant alignment and rotational revivals in iodine molecules. The same alignment technique may be applicable, in favourable cases, to study the stereodynamics of bimolecular reactions. One should note that alignment revivals created in this way differ from the alignment created by strong (quasi)static fields (the so-called pendular states) in that the alignment persists, in the sense that it recurs, after the orienting field is removed.

In conclusion, we believe that recent advances in detector and laser technology have opened a door into an unexplored wing in the mansion house of molecular reaction dynamics. There is much to investigate. Time-resolved pump–probe experiments with ultrafast lasers coupled to CPI methods allow us to study non-adiabatic interactions in molecular systems with unprecedented resolution. We have in effect a molecular microscope with which to examine the details of both the electronic and the nuclear wavefunctions as a molecule is transformed. The technology also has the potential to allow us to manipulate ensembles of molecules so that we can spin them in space and control their orientation. This then will allow us to study the stereochemistry of the transformation. What is more the technology allows us to study the details of the chemistry of much larger molecules than has traditionally been the realm of molecular reaction dynamics. We have well and truly moved beyond the 'age of the alkali metals' that characterized the early days of the field nearly 50 years ago.

Acknowledgements

B.J.W. is grateful to the Ministry of Education, Science, Sports and Culture of Japan for a visiting fellowship to the Institute for Molecular Science. Financial support to T.S. through the Grant-in-Aid from the Ministry of Education, Science, Sports, and Culture under contracts 11359005 and 11440183 is also gratefully

acknowledged. Some of the work described here has been supported by the European Union under contract ERB 4061 PL 97-0264.

References

AHMED, M., PETERKA, D. S., BRACKER, A. S., VASYUTINSKII, O. S., and SUITS, A. G., 1999, *J. chem. Phys.*, **110**, 4115.

ALTHORPE, S. C., and SEIDEMAN, T., 1999, *J. chem. Phys.*, **110**, 147.

AMATATSU, Y., YABUSHITA, S., and MOROKUMA, K., 1996, *J. chem. Phys.*, **104**, 9783.

AMITAY, Z., and ZAJFMAN, D., 1997, *Rev. Scient. Instrum.*, **68**, 1387.

ANDRESEN, P., and ROTHE, E. W., 1983, *J. chem. Phys.*, **78**, 989.

ARASAKI, Y., TAKATSUKA, K., WANG, K., and MCKOY, V., 2000, *J. chem. Phys.*, **112**, 8871.

AVOURIS, P., GELBERT, W. M., and EL-SAYED, M. A., 1977, *Chem. Rev.*, **77**, 793.

BACKUS, S., DURFEE, C. G., MURNANE, M. M., and KAPTEYN, H. C., 1998, *Rev. Scient. Instrum.*, **69**, 1207.

BAER, T., and HASE, W. L., 1996. *Unimolecular Reaction Dynamics, Theory and Experiments* (Oxford University Press).

BANDRAUK, A. D., AUBANEL, E. E., and GAUTHIER, J.-M. 1993, *Molecules in Intense Laser Fields*, edited by A. D. Bandrauk (New York: Marcel Dekker), pp. 109–179.

BANDRAUK, A. D., CHELKOWSKI, S., and CORKUM, P. B., 1999, *Int. J. quant. Chem.*, **75**, 951.

BARTY, C. P. J., GUO, T., LEBLANC, C., RAKSI, F., ROSE-PETRUCK, C. G., SQUIER, J. A., WALKER, B. C., WILSON, K. R., YAKOVLEV, V. V., and YAMAKAWA, K. 1996, *Sub-20-fs Multiterawatt Lasers and X-ray Applications* in *X-Ray Lasers* (Bristol: Institute of Physics), p. 282.

BASKIN, J. S., FELKER, P. M., and ZEWAIL, A. H., 1987, *J. chem. Phys.*, **86**, 2483.

BELBRUNO, J. J., 1995, *Int. Rev. phys. Chem.*, **14**, 67.

BERSOHN, R., 1975, *Israel J. Chem.*, **14**, 111; 1984, *J. phys. Chem.*, **88**, 5145.

BERSOHN, R., and LIN, S. H., 1969, *Adv. chem. Phys.*, **16**, 80.

BETHE, H. A., 1933, *Handbuch der Physik*, Vol. 24 (Berlin: Springer), p. 483.

BIXON, M., and JORTNER, J., 1968, *J. chem. Phys.*, **48**, 715.

BLANCHET, V., ZGIERSKI, M. Z., SEIDEMAN, T., and STOLOW, A., 1999, *Nature*, **401**, 52.

BLUNT, D. A., and SUITS, A. G., 1997, *Highly Excited Molecules*, ACS Symposium Series, Vol. 678 (Washington, DC: American Chemical Society), p. 99.

BONTUYAN, L. S., SUITS, A. G., HOUSTON, P. L., and WHITAKER, B. J., 1993, *J. phys. Chem.*, **97**, 6342.

BORDAS, C., 1998, *Phys. Rev.* A, **58**, 400.

BORDAS, C., DYER, M. J., FAIRFIELD, T., HELM, H., and KULANDER, K. C., 1995, *Phys. Rev.* A, **51**, 3726.

BORDAS, C., DYER, M. J., FAIRFIELD, T. A., SAEED, M., and HELM, H., 1994, *J. Phys., Paris*, **4**, 647.

BORDAS, C., PAULIG, F., HELM, H., and HUESTIS, D. L., 1996, *Rev. Scient. Instrum.*, **67**, 2257.

BORDAS, C., and PINARE, J. C., 1998, *Phys. Rev.* A, **57**, R681.

BRACKER, A. S., WOUTERS, E. R., SUITS, A. G., and VASYUTINSKII, O. S., 1999, *J. chem. Phys.*, **110**, 6749.

BRAUN, M., MEIER, C., and ENGEL, V., 1996, *J. chem. Phys.*, **105**, 530.

BRENOT, J. C., and DURUP-FERGUSON, M., 1992, *Adv. chem. Phys.*, **82**, 309.

BREWCZYK, M., and RZAZEWSKI, K., 1999, *Phys. Rev.* A, **60**, 2285.

BUDINGER, T. F., and GULLBERG, G. T., 1974, *IEEE Trans. nucl. Sci.*, **2**, NS–21.

BUNTINE, M. A., BALDWIN, D. P., ZARE, R. N., and CHANDLER, D. W., 1991, *J. chem. Phys.*, **94**, 4672.

BUSH, G. E., and WILSON, K. R., 1972, *J. chem. Phys.*, **56**, 3626.

BUTLER, L. J., 1998, *A. Rev. phys. Chem.*, **49**, 125.

CAO, J. M., IHEE, H., and ZEWAIL, A. H., 1999, *Proc. natn. Acad. Sci. USA*, **96**, 338.

CASAVECCHIA, P., 2000, *Rep. Prog. Phys.*, **63**, 355.

CATALAN, J., DEL VALLE, J. C., and KASHA, M., 2000, *Chem. Phys. Lett.*, **318**, 629.

CHANDLER, D. W., and HOUSTON, P. L., 1987, *J. chem. Phys.*, **87**, 1445.

CHANDLER, D. W., JANSSEN, M. H. M., STOLTE, S., STRICKLAND, R. N., THOMAN, J. W., and PARKER, D. H., 1990, *J. phys. Chem.*, **94**, 4839.
CHANDLER, D. W., and PARKER, D. H., 1999. *Adv. Photochem.*, **25**, 59.
CHANDLER, D. W., THOMAN, J. W., JANSSEN, M. H. M., and PARKER, D. H., 1989, *Chem. Phys. Lett.*, **156**, 151.
CHANDRA, N., and CHAKRABORTY, M., 1991, *J. chem. Phys.*, **95**, 6382.
CHANG, B. Y., HOETZLEIN, R. C., MUELLER, J. A., GEISER, J. D., and HOUSTON, P. L., 1998, *Rev. Scient. Instrum.*, **69**, 1665.
CHARRON, E., and SUZOR-WEINER, A., 1998, *J. chem. Phys.*, **108**, 3922.
CHELKOWSKI, S., CORKUM, P. B., and BANDRAUK, A. D., 1999, *Phys. Rev. Lett.*, **82**, 3416.
CHEREPKOV, N. A., 1983, *Adv. at. molec. Phys.*, **19**, 395.
CHUPKA, W. A., 1993, *J. chem. Phys.*, **98**, 4520.
CODLING, K., and FRASINSKI, L. J., 1994, *Contemp. Phys.*, **35**, 243.
CONSTANT, E., STAPELFELDT, H., and CORKUM, P. B., 1996, *Phys. Rev. Lett.*, **76**, 4140.
COOK, P. A., LANGFORD, S. R., ASHFOLD, M. N. R., and DIXON, R. N., 2000, *J. chem. Phys.*, **113**, 994.
COOPER, J., and ZARE, R. N., 1968, *J. chem. Phys.*, **48**, 942.
COOPER, M. J., JACKSON, P. J., ROGERS, L. J., ORR-EWING, A. J., and WHITAKER, B. J., 1998, *J. chem. Phys.*, **109**, 4367.
CORKUM, P. B., ELLERT, C., MEHENDALE, M., DIETRICH, P., HANKIN, S., ASEYEV, S., RAYNER, D., and VILLENEUVE, D., 1999, *Discuss. Faraday Soc.*, **113**, 47.
CORKUM, P. B., IVANOV, M. Y., and WRIGHT, J. S., 1997, *A. Rev. phys. Chem.*, **48**, 387
CORNAGGIA, C., 1995, *Phys. Rev.* A, **52**, R4328.
CORNAGGIA, C., SCHMIDT, M., and NORMAND, D., 1994, *J. Phys.* B, **27**, L 123.
DAVIES, J. A., LECLAIRE, J. E., CONTINETTI, R. E., and HAYDEN, C. C., 1999, *J. chem. Phys.*, **111**, 1.
DE LANGE, P. J., DRABE, K. E., and KOMMANDEUR, J., 1986, *J. chem. Phys.*, **84**, 538.
DELONE, N. B., and KRAINOV, V. P., 1994. *Multiphoton Processes in Atoms* (Berlin: Springer).
DESHMUKH, S., and HESS, W. P., 1994, *J. chem. Phys.*, **100**, 6429.
DIETRICH, P., STRICKLAND, D. T., LABERGE, M., and CORKUM, P. B., 1993, *Molecules in Laser Fields*, edited by A. D. Bandrauk (New York: Marcel Dekker).
DILL, D., 1976, *J. chem. Phys.*, **65**, 1130.
DILL, D., SIEGEL, J., and DEHMER, J. L., 1976, *J. chem. Phys.*, **65**, 3158.
DOUHAL, A., KIM, S. K., and ZEWAIL, A. H., 1995, *Nature*, **378**, 260.
DOWNIE, P., and POWIS, I., 1999a, *J. Chem. Phys.*, **111**, 4535; 1999b, *Phys. Rev. Lett.*, **82**, 2864.
DOWNIE, P., and REYNOLDS, D. J., POWIS, I., 1995, *Rev. scient. Instrum.*, **66**, 3807.
DRABBELS, M., MORGAN, C. G., MCGUIRE, D. S., and WODTKE, A. M., 1995, *J. chem. Phys.*, **102**, 611.
ELLERT, C., STAPELFELDT, H., CONSTANT, E., SAKAI, H., WRIGHT, J., RAYNER, D. M., and CORKUM, P. B., 1998, *Phil. Trans. R. Soc.* A, **356**, 329.
ENGEL, V., and METIU, H., 1989a, *J. chem. Phys.*, **90**, 6116; 1989b, *Chem. Phys. Lett.*, **155**, 77.
EPPINK, A., and PARKER, D. H., 1997, *Rev. Scient. Instrum.*, **68**, 3477; 1999, *J. chem. Phys.*, **110**, 832.
FELKER, P. M., and ZEWAIL, A. H., 1986, *Chem. Phys. Lett.*, **128**, 221; 1987, *J. chem. Phys.*, **86**, 2460.
FERNÁNDEZ-ALONSO, F., BEAN, B. D., AYERS, J. D., POMERANTZ, A. E., ZARE, R. N., BAÑARES, L., and AOIZ, F. J., 2000, *Angew. Chem., Int. Edn*, **39**, 2748.
FOLMER, D. E., POTH, L., WISNIEWSKI, E. S., and CASTLEMAN, A. W., 1998, *Chem. Phys. Lett.*, **287**, 1.
FOLMER, D. E., WISNIEWSKI, E. S., and CASTLEMAN, A. W., 2000, *Chem. Phys. Lett.*, **318**, 637.
FOLMER, D. E., WISNIEWSKI, E. S., HURLEY, S. M., and CASTLEMAN, A. W., 1999, *Proc. natn. Acad. Sci. USA*, **96**, 12 980.
FRAD, A., LAHMANI, F., TRAMER, A., and TRIC, C., 1974, *J. chem. Phys.*, **60**, 4419.
FRASINSKI, L. J., HATHERLY, P. A., and CODLING, K., 1991, *Phys. Lett.* A, **156**, 227.

FRASINSKI, L. J., STANKIEWICZ, M., HATHERLY, P. A., CROSS, G. M., CODLING, K., LANGLEY, A. J., and SHAIKH, W., 1992, *Phys. Rev.* A, **46**, R6789.

FRISCH, M. J., TRUCKS, G. W., SCHLEGEL, H. B., SCUSERIA, G. E., ROBB, M. A., CHEESEMAN, J. R., ZAKRZEWSKI, V. G., MONTGOMERY, J. A., STRATMANN, R. E., BURANT, J. C., DAPPRICH, S., MILLAM, J. M., DANIELS, A. D., KUDIN, K. N., STRAIN, M. C., FARKAS, O., TOMASI, J., BARONE, V., COSSI, M., CAMMI, R., MENNUCCI, B., POMELLI, C., ADAMO, C., CLIFFORD, S., OCHTERSKI, J., PETERSSON, G. A., AYALA, P. Y., CUI, Q., MOROKUMA, K., MALICK, D. K., RABUCK, A. D., RAGHAVACHARI, K., FORESMAN, J. B., CIOSLOWSKI, J., ORTIZ, J. V., STEFANOV, B. B., LIU, G., LIASHENKO, A., PISKORZ, P., KOMAROMI, I., GOMPERTS, R., MARTIN, R. L., FOX, D. J., KEITH, R., AL-LAHAM, M. A., PENG, C. Y., NANAYAKKARA, A., GONZALEZ, C., CHALLACOMBE, M., GILL, P. M. W., JOHNSON, B. G., CHEN, W., WONG, M. W., ANDRES, J. L., HEAD-GORDON, M., REPLOGLE, E. S., and POPLE, J. A., 1998, *Gaussian98* (Gaussian, Inc.).

GLASS-MAUJEAN, M., and BESWICK, J. A., 1989, *J. chem. Soc., Faraday Trans.*, **85**, 983.

GOLOVIN, A. V., 1991, *Optika i Spektrosk.*, **71**, 933; 1998, *J. Electron Spectrosc. Relat. Phenomena*, **96**, 117.

GOLOVIN, A. V., and CHEREMNYKH, P. G., 1991, *Instrum. Exp. Tech.*, **34**, 385.

HALL, G. E., and HOUSTON, P. L., 1989, *A. Rev. phys. Chem.*, **40**, 375.

HATHERLY, P. A., ADACHI, J., SHIGEMASA, E., and YAGISHITA, A., 1995, *J. Phys.* B, **28**, 2643.

HECK, A. J. R., 1997, *Eur. Mass Spectrom.*, **3**, 171.

HECK, A. J. R., and CHANDLER, D. W., 1995, *A. Rev. phys. Chem.*, **46**, 335.

HELM, H., BJERRE, N., DYER, M. J., HUESTIS, D. L., and SAEED, M., 1993, *Phys. Rev. Lett.*, **70**, 3221.

HERING, P., and CORNAGGIA, C., 1999, *Phys. Rev.* A, **59**, 2836.

HISHIKAWA, A., IWAMAE, A., HOSHINA, K., KONO, M., and YAMANOUCHI, K., 1998a, *Chem. Phys.* **231**, 315; 1998b, *Chem. Phys. Lett.*, **282**, 283.

HOLBROOK, K. A., PILLING, M. J., and ROBERTSON, S. H., 1996. *Unimolecular Reactions* (New York: Wiley).

HOLTZCLAW, K. W., SPANGLER, L. H., and PRATT, D. W., 1989, *Chem. Phys. Lett.*, **161**, 347.

HOUSTON, P. L., 1995, *Accts Chem. Res.*, **28**, 453.

INNES, K. K., ROSS, I. G., and MOOMAW, W. R., 1988, *J. molec. Spectrosc.*, **132**, 492.

JOHNSON, B. R., KITTRELL, C., KELLY, P. B., and KINSEY, J. L., 1996, *J. phys. Chem.*, **100**, 7743.

JONAH, C., 1971, *J. chem. Phys.*, **55**, 1915.

JOUVET, C., MARTRENCHARD, S., SOLGADI, D., DEDONDER-LARDEUX, C., MONS, M., GREGOIRE, G., DIMICOLI, I., PIUZZI, F., VISTICOT, J. P., MESTDAGH, J. M., DOLIVEIRA, P., MEYNADIER, P., and PERDRIX, M., 1997, *J. chem. Phys.* A, **101**, 2555.

JUNG, Y. J., KIM, Y. S., KANG, W. K., and JUNG, K. H., 1997, *J. chem. Phys.*, **107**, 7187.

KAESDORF, S., SCHONHENSE, G., and HEINZMANN, U., 1985, *Phys. Rev. Lett.*, **54**, 885.

KANG, W. K., KIM, Y. S., and JUNG, K. H., 1995, *Chem. Phys. Lett.*, **244**, 183.

KATAYANAGI, H., MO, Y. X., and SUZUKI, T., 1995, *Chem. Phys. Lett.*, **247**, 571.

KELDYSH, L. V., 1964, *Zh. eksp. teor. Fiz.*, **47**, 1945 (Engl. Transl., 1965, *Soviet Phys. JETP*, **20**, 1307).

KELLA, D., ALGRANATI, M., FELDMAN, H., HEBER, O., KOVNER, H., MALKIN, E., MIKLAZKY, E., NAAMAN, R., ZAJFMAN, D., ZAJFMAN, J., and VAGER, Z., 1993, *Nucl. Instrum. Meth.*, **329**, 440.

KENDRICK, B. K., JAYASINGHE, L., MOSER, S., AUZINSH, M., and SHAFER-RAY, N., 2000, *Phys. Rev. Lett.*, **84**, 4325.

KIM, S. K., GUO, J., BASKIN, J. S., and ZEWAIL, A. H., 1996, *J. phys. Chem.*, **100**, 9202.

KIM, S. K., PEDERSEN, S., and ZEWAIL, A. H., 1995, *J. chem. Phys.*, **103**, 477.

KIM, S. K., and ZEWAIL, A. H., 1996, *Chem. Phys. Lett.*, **250**, 279.

KIM, W., and FELKER, P. M., 1996, *J. chem. Phys.*, **104**, 1147.

KIM, Z. H., ALEXANDER, A. J., KANDEL, S. A., RAKITZIS, T. P., and ZARE, R. N., 1999, *Discuss. Faraday Soc.*, **113**, 27.

KITSOPOULOS, T. N., BUNTINE, M. A., BALDWIN, D. P., ZARE, R. N., and CHANDLER, D. W., 1993, *Science*, **260**, 1605.
KNEE, J. L. 1995, *High Resolution Photoionisation and Photoelectron Studies*, edited by I. Powis, T. Baer and C. Y. Ng (New York: Wiley), pp. 369–406.
KNEE, J. L., DOANY, F. E., and ZEWAIL, A. H., 1985, *J. chem. Phys.*, **82**, 1042.
KRUIT, P., and READ, F. H., 1983, *J. Phys.* E, **16**, 313.
KUPRIYANOV, D. V., and VASYUTINSKII, O. S., 1993, *Chem. Phys.* **171**, 25.
LAHMANI, F., TRAMER, A., and TRIC, C., 1974, *J. chem. Phys.*, **60**, 4431.
LARSEN, J. J., MORKBAK, N. J., OLESEN, J., BJERRE, N., MACHHOLM, M., KEIDING, S. R., and STAPELFELDT, H., 1998, *J. chem. Phys.*, **109**, 8857.
LEAHY, D. J., REID, K. L., PARK, H. K., and ZARE, R. N., 1992, *J. chem. Phys.*, **97**, 4948.
LEVIN, J., FELDMAN, H., BAER, A., BEN-HAMU, D., HEBER, O., ZAJFMAN, D., and VAGER, Z., 1998, *Phys. Rev. Lett.*, **81**, 3347.
LEVIN, J., KELLA, D., and VAGER, Z., 1996, *Phys. Rev.* A, **53**, 1469.
LEVIN, J., KNOLL, L., SCHEFFEL, M., SCHWALM, D., WESTER, R., WOLF, A., BAER, A., VAGER, Z., ZAJFMAN, D., and LIECHTENSTEIN, V. K., 2000, *Nucl. Instrum. Meth.*, **168**, 268.
LEVINE, R. D., and BERNSTEIN, R. B., 1987. *Molecular Reaction Dynamics and Chemical Reactivity* (Oxford University Press).
LIU, X., LIN, J. J., HARICH, S., SCHATZ, G. C., and YANG, X., 2000, *Science*, **289**, 1536.
LOCKER, J. R., BURKHOLDER, J. B., BAIR, E. J., and WEBSTER, H. A., 1983, *J. phys. Chem.*, **87**, 1864.
LOESCH, H. J., 1995, *A. Rev. phys. Chem.*, **46**, 555.
LORENZ, K. T., WESTLEY, M. S., and CHANDLER, D. W., 2000, *Phys. Chem. Chem. Phys.*, **2**, 481.
LORINCZ, A., SMITH, D. D., NOVAK, F., KOSLOFF, R., TANNOR, D. J., and RICE, S. A., 1985, *J. chem. Phys.*, **82**, 1067.
MARTINEZ-NUNEZ, E., and VAZQUEZ, S. A., 2000, *Chem. Phys. Lett.*, **316**, 471.
MCDONALD, D. B., FLEMING, G. R., and RICE, S. A., 1981, *Chem. Phys.* **60**, 335.
MO, Y. X., KATAYANAGI, H., HEAVEN, M. C., and SUZUKI, T., 1996, *Phys. Rev. Lett.*, **77**, 830.
MO, Y. X., KATAYANAGI, H., and SUZUKI, T., 1999, *J. chem. Phys.*, **110**, 2029.
MO, Y. X., and SUZUKI, T., 1998, *J. chem. Phys.*, **108**, 6780.
MORGAN, C. G., DRABBELS, M., and WODTKE, A. M., 1996, *J. chem. Phys.*, **105**, 4550.
MÜLLER-DETHLEFS, K., and SCHLAG, E. W., 1991, *A. Rev. phys. Chem.*, **42**, 109.
NEUMARK, D. M., 1992, *A. Rev. phys. Chem.*, **43**, 153.
NICOLE, C., SLUIMER, I., ROSCA-PRUNA, F., WARNTJES, M., VRAKKING, M., BORDAS, C., TEXIER, F., and ROBICHEAUX, F., 2000, *Phys. Rev. Lett.*, **85**, 4024.
NORTH, S. W., BLANK, D. A., and LEE, Y. T., 1994, *Chem. Phys. Lett.*, **28**, 224.
OKAJIMA, S., SAIGUSA, H., and LIM, E., 1982, *J. chem. Phys.*, **76**, 2096.
ONDREY, G. S., KANFER, S., and BERSOHN, R., 1983, *J. chem. Phys.*, **79**, 179.
OWRUTSKY, J. C., and BARONAVSKI, A. P., 1999, *J. chem. Phys.*, **111**, 7329.
PALLIX, J. B., and COLSON, S. D., 1985, *Chem. Phys. Lett.*, **119**, 38.
PERSON, M. D., KASH, P. W., and BUTLER, L. J., 1992, *J. chem. Phys.*, **97**, 355.
PINARE, J. C., BAGUENARD, B., BORDAS, C., and BROYER, M., 1998, *Phys. Rev. Lett.*, **81**, 2225; 1999, *Eur. Phys. J.* D, **9**, 21.
POLANYI, J. C., 1987, *Science*, **236**, 680.
POLANYI, J. C., and ZEWAIL, A. H., 1995, *Accts Chem. Res.*, **28**, 119.
POSTHUMUS, J. H., GILES, A. J., THOMPSON, M., SHAIKH, W., LANGLEY, A. J., FRASINSKI, L. J., and CODLING, K., 1996, *J. Phys.* B, **29**, L 525.
POWIS, I., BAER, T., and NG, C. Y. (editors), 1995, *High Resolution Photoionisation and Photoelectron Studies* (New York: Wiley).
PRATT, D. W., 1998, *A. Rev. phys. Chem.*, **49**, 481.
RAKITZIS, T. P., HALL, G. E., COSTEN, M. L., and ZARE, R. N., 1999a, *J. chem. Phys.*, **111**, 8751.
RAKITZIS, T. P., SAMARTZIS, P. C., and KITSOPOULOS, T. N., 1999b, *J. chem. Phys.*, **111**, 10 415.
RAKITZIS, T. P., and ZARE, R. N., 1999, *J. chem. Phys.*, **110**, 3341.

RAKSI, F., WILSON, K. R., JIANG, Z. M., IKHLEF, A., COTE, C. Y., and KIEFFER, J. C., 1996, *J. chem. Phys.*, **104**, 6066.
REID, G. D., and WYNNE, K. 2000, 'Ultrafast laser technology and spectroscopy' in *Encyclopedia of Analytical Chemistry*, edited by R. A. Myers (New York: Wiley)
REID, K. L., FIELD, T. A., TOWRIE, M., and MATOUSEK, P., 1999, *J. chem. Phys.*, **111**, 1438.
REID, K. L., and UNDERWOOD, J. G., 2000, *J. chem. Phys.*, **112**, 3643.
REISS, H. R., 1980, *Phys. Rev.* A, **22**, 1786.
RINNEN, K. D., KLINER, D. A. V., BLAKE, R. S., and ZARE, R. N., 1989, *Rev. Scient. Instrum.*, **60**, 717.
ROSE, T. S., ROSKER, M. J., and ZEWAIL, A. H., 1988, *J. chem. Phys.*, **88**, 6672; 1989, *ibid*, **91**, 7415.
ROSEN, S., PEVERALL, R., TER HORST, J., SUNDSTROM, G., SEMANIAK, J., SUNDQVIST, O., LARSSON, M., DE WILDE, M., and VAN DER ZANDE, W. J., 1998, *Hyperfine Interact.*, **115**, 201.
ROSKER, M. J., DANTUS, M., and ZEWAIL, A. H., 1988, *J. chem. Phys.*, **89**, 6113.
SAEED, M., DYER, M. J., and HELM, H., 1994, *Phys. Rev.* A, **49**, 1491.
SAKAI, H., SAFVAN, C. P., LARSEN, J. J., HILLIGSOE, K. M., HALD, K., and STAPELFELDT, H., 1999, *J. chem. Phys.*, **110**, 10 235.
SATO, Y., MATSUMI, M., KAWASAKI, M., TSUKIYAMA, K., and BERSOHN, R., 1995a, *J. phys. Chem.*, **99**, 16 307; 1995b, *ibid.*, **99**, 16 307.
SCHNIEDER, L., SEEKAMP-RAHN, K., BORKOWSKI, J., WREDE, E., WELGE, K. H., AOIZ, F. J., BANARES, L., D'MELLO, M. J., HERRERO, V. J., RABANOS, V. S., and WYATT, R. E., 1995, *Science*, **269**, 207.
SCHNIEDER, L., SEEKAMPRAHN, K., WREDE, E., and WELGE, K. H., 1997, *J. chem. Phys.*, **107**, 6175.
SEEL, M., and DOMCKE, W., 1991, *Chem. Phys.* **151**, 59.
SEIDEMAN, T., 1997, *J. chem. Phys.*, **107**, 7859; 1999, *Phys. Rev. Lett.*, **83**, 4971.
SEKRETA, E., and REILLY, J. P., 1988, *Chem. Phys. Lett.*, **149**, 482.
SHIBATA, T., and SUZUKI, T., 1996, *Chem. Phys. Lett.*, **262**, 115.
SIEBBELES, L. D. A., GLASSMAUJEAN, M., VASYUTINSKII, O. S., BESWICK, J. A., and RONCERO, O., 1994, *J. chem. Phys.*, **100**, 3610.
SIMONS, J. P., 1999, *Discuss. Faraday Soc.*, **113**, 1.
SIVAKUMAR, N., HALL, G. E., HOUSTON, P. L., HEPBURN, J. W., and BURAK, I., 1988, *J. chem. Phys.*, **88**, 3692.
SKODJE, R. T., SKOUTERIS, D., MANOLOPOULOS, D. E., LEE, S.-H., DONG, F., and LIU, K., 2000, *Phys. Rev. Lett.*, **85**, 1206.
STAPELFELDT, H., CONSTANT, E., and CORKUM, P. B., 1995, *Phys. Rev. Lett.*, **74**, 3780.
STERT, V., FARMANARA, P., and RADLOFF, W., 2000, *J. chem. Phys.*, **112**, 4460.
STOLOW, A., 1999, *Abstr. Papers. Am. chem. Soc.*, **217**, 344.
SUITS, A. G., BONTUYAN, L. S., HOUSTON, P. L., and WHITAKER, B. J., 1992, *J. chem. Phys.*, **96**, 8618.
SUITS, A. G., MILLER, R. L., BONTUYAN, L. S., and HOUSTON, P. L., 1993, *J. chem. Soc., Faraday Trans.*, **89**, 3667.
SUZUKI, T., KATAYANAGI, H., NANBU, S., and AOYAGI, M., 1998, *J. chem. Phys.*, **109**, 5778.
SUZUKI, T., WANG, L., and KOHGUCHI, H., 1999, *J. chem. Phys.*, **111**, 4859.
TAKAHASHI, M., CAVE, J. P., and ELAND, J. H. D., 2000, *Rev. Scient. Instrum.*, **71**, 1337.
TAYLOR, C. A., EL BAYOUMI, M. A., and KASHA, M., 1969, *Proc. natn. Acad. Sci. USA*, **63**, 253.
TELLINGHUISEN, J., 1973, *J. chem. Phys.*, **58**, 2821.
THOMAN, J. W., CHANDLER, D. W., PARKER, D. H., and JANSSEN, M. H. M., 1988, *Laser Chem.*, **9**, 27.
TSUBOUCHI, M., WHITAKER, B. J., WANG, L., KOHGUCHI, H., and SUZUKI, T., 2001, *Phys. Rev. Lett.*, **86**, 4500.
UNDERWOOD, J. G., and POWIS, I., 2000, *J. chem. Phys.*, **113**, 7119.
UNDERWOOD, J. G., and REID, K. L., 2000, *J. Chem. Phys.*, **113**, 1067.
VAGER, Z., NAAMAN, R., and KANTER, E. P., 1989, *Science*, **244**, 426.

VAN BRUNT, R. J., and ZARE, R. N., 1968, *J. chem. Phys.*, **48**, 4304.
VAN DER MEER, B. J., JONKMAN, H. T., KOMMANDEUR, J., MEERTS, W. L., and MAJEWSKI, W. A., 1982, *Chem. Phys. Lett.*, **92**, 565.
VRAKKING, M., 2001, *Phys. Rev. Lett.* (submitted).
WANG, K. S., and MCKOY, V., 1995, *A. Rev. phys. Chem.*, **46**, 275.
WANG, L., KOHGUCHI, H., and SUZUKI, T., 1999, *Discuss. Faraday Soc.*, **113**, 37.
WHITAKER, B. J., 1993, *Research in Chemical Kinetics*, Vol. 1, edited by R. G. Compton, and G. Hancock (Amsterdam: Elsevier); 2000, *Image Reconstruction: the Abel Transform* in *Imaging in Chemical Dynamics*, ACS Symposium Series, Vol. 770, edited by A. G. Suits and R. E. Continetti (Washington, DC: American Chemical Society).
WILEY, W. C., and MCLAREN, I. H., 1955, *Rev. scient. Instrum.*, **60**, 1150.
WILLIAMSON, J. C., CAO, J. M., IHEE, H., FREY, H., and ZEWAIL, A. H., 1997, *Nature*, **386**, 159.
WINTERHALTER, J., MAIER, D., HONERKAMP, J., SCHYJA, V., and HELM, H., 1999, *J. chem. Phys.*, **110**, 11187.
WREDE, E., LAUBACH, S., SCHULENBURG, S., ORR-EWING, A. J., and ASHFOLD, M. N. R., 2000, *Chem. Phys. Lett.*, **326**, 22.
YAMAZAKI, I., MURAO, T., YAMANAKA, T., and YOSHIHARA, K., 1983, *Discuss. Faraday Soc.*, 395.
YANG, C. N., 1948, *Phys. Rev.*, **74**, 764.
YANG, S., and BERSOHN, R., 1974, *J. chem Phys*., **61**, 4400.
YONEKURA, N., GEBAUER, C., KOHGUCHI, H., and SUZUKI, T., 1999, *Rev. Scient. Instrum.*, **70**, 3265.
ZAJFMAN, D., KANTER, E. P., GRABER, T., VAGER, Z., and NAAMAN, R., 1992, *Nucl. Instrum. Meth*., **67**, 22.
ZARE, R. N., 1972, *Molec. Photochem.*, **4**, 1.
ZEWAIL, A. H., 1996, *J. phys. Chem.*, **100**, 12 701; 1997, *Adv. chem. Phys.*, **101**, 892; 2000, *J. chem. Phys.* A, **104**, 5660.